RESEARCH ARTICLE | NOVEMBER 27 2024

A reaction network model of microscale liquid–liquid phase separation reveals effects of spatial dimension ☐

Special Collection: 2024 JCP Emerging Investigators Special Collection

Jinyoung Kim ; Sean D. Lawley ; Jinsu Kim ☐

J. Chem. Phys. 161, 204110 (2024)
https://doi.org/10.1063/5.0235456

The Journal of Chemical Physics ARTICLE pubs.aip.org/aip/jcp

A reaction network model of microscale liquid–liquid phase separation reveals effects of spatial dimension

Cite as: J. Chem. Phys. 161, 204110 (2024); doi: 10.1063/5.0235456
Submitted: 27 August 2024 • Accepted: 28 October 2024 •
Published Online: 27 November 2024

Jinyoung Kim, [1] Sean D. Lawley, [2] and Jinsu Kim [1, a)]

AFFILIATIONS

[1]Department of Mathematics, Pohang University of Science and Technology (POSTECH), Pohang 37673, Republic of Korea
[2]Department of Mathematics, University of Utah, Salt Lake City, Utah 84112, USA

Note: This paper is part of the 2024 JCP Emerging Investigators Special Collection.
[a)]Author to whom correspondence should be addressed: jinsukim@postech.ac.kr

ABSTRACT

Proteins can form droplets via liquid–liquid phase separation (LLPS) in cells. Recent experiments demonstrate that LLPS is qualitatively different on two-dimensional (2D) surfaces compared to three-dimensional (3D) solutions. In this paper, we use mathematical modeling to investigate the causes of the discrepancies between LLPS in 2D and 3D. We model the number of proteins and droplets inducing LLPS by continuous-time Markov chains and use chemical reaction network theory to analyze the model. To reflect the influence of space dimension, droplet formation and dissociation rates are determined using the first hitting times of diffusing proteins. We first show that our stochastic model reproduces the appropriate phase diagram and is consistent with the relevant thermodynamic constraints. After further analyzing the model, we find that it predicts that the space dimension induces qualitatively different features of LLPS, which are consistent with recent experiments. While it has been claimed that the differences between 2D and 3D LLPS stem mainly from different diffusion coefficients, our analysis is independent of the diffusion coefficients of the proteins since we use the stationary model behavior. Our results thus give new hypotheses about how space dimension affects LLPS.

I. INTRODUCTION

In a cell, liquid–liquid phase separation (LLPS) manifests as the formation of droplets from protein condensation. These liquid droplets in a dense phase separate from their surrounding spaces of dilute phases.[1–5] Biologists have made significant strides in elucidating the importance of LLPS and its involvement in cellular processes. Repair protein factors, for example, are involved in the initiation of LLPS during DNA double-strand breaks.[6–8] In addition, it has been found that the condensates of SCOTIN, an Endoplasmic Reticulum (ER) transmembrane protein with a cytosolic intrinsically disordered region, inhibit ER-to-Golgi transport through LLPS.[9] Furthermore, dysregulation of LLPS has been associated with various diseases, including cancer.[10–12]

LLPS is found in many different intracellular locations, including on two-dimensional (2D) surfaces such as the endoplasmic reticulum membrane[9,13,14] or in three-dimensional (3D) spaces such as the cytoplasm[13,15–17] [Fig. 1(a)]. Qualitative differences between two-dimensional LLPS (2D-LLPS) and three-dimensional LLPS (3D-LLPS) have been observed recently.[14,18,19] For example, Snead *et al.*[14] revealed differences in droplet formation times between 2D and 3D environments. While droplets in 2D can form within minutes, it takes hours for them to form in 3D. In addition, droplets in 2D can be arrested within minutes, suggesting resistance to size growth, whereas in 3D, they can reach their maximum size within hours. To explain these qualitative differences observed in 2D vs 3D, some have proposed that droplet size arrest may result from disparities of diffusion coefficients in 2D and 3D environments.[14] For example, diffusion coefficients of eGFP proteins in 2D differ markedly from 3D.[20,21]

While it is true that diffusion coefficients differ in 2D vs 3D cellular environments, the space dimension has more fundamental effects on diffusion processes. For example, far fewer steps are required (on average) for a random walk to find a target if the

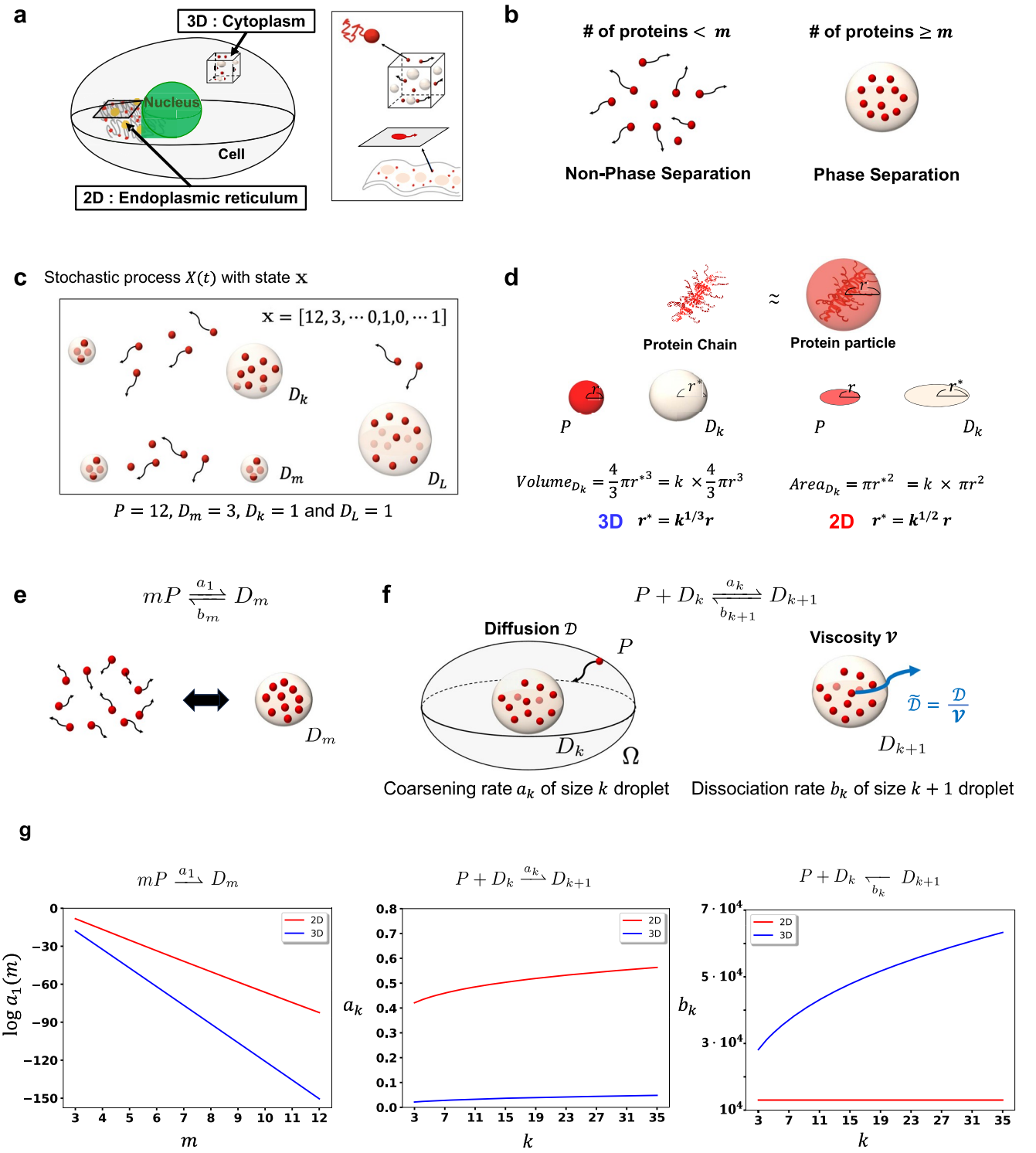

FIG. 1. Overview of modeling LLPS using a reaction network. (a) LLPS occurrence in 2D (e.g., membrane) and 3D (e.g., cytoplasm). (b) The value m represents the threshold number required for droplet formation. (c) A visual representation of a state of the Markov chain $X(t)$. (d) The hydrodynamic radius r of a protein. A droplet is approximated as a sphere in 3D and a circle in 2D to derive its radius. (e) and (f) Understanding the reaction rates a_1, a_k's and b_k's. The a_k and b_k are defined by mean first hitting and exit times. (g) Plots of the rates a_1, a_k, b_k of 2D and 3D under equal diffusion coefficients and viscosity.

search is restricted to a 2D lattice rather than a 3D lattice.[22] More mathematically sophisticated examples of dimensional discrepancies include the recurrence vs transience of 2D vs 3D random walks[23,24] and the logarithmic vs algebraic singularities of the 2D vs 3D Laplacian Green's functions.[25] Importantly, these discrepancies cannot be accounted for by merely rescaling time. Studying how these fundamental dimensional differences in diffusion affect cell biology has a long history in the biophysics literature.[26–37] How do these differences affect LLPS?

In this paper, we formulate and analyze the mathematical models of microscopic intracellular LLPS and theoretically compare LLPS in 2D vs 3D. The main theoretical framework for this is biochemical reaction network theory.[38] By describing droplet formation, coarsening, and dissociation with reactions between species, LLPS can be associated with a reaction network. Our model consists of the following reactions:

$$\begin{aligned} &mP \underset{b_m}{\overset{a_m}{\rightleftarrows}} D_m \quad (\text{droplet formation}),\\ &P + D_k \underset{b_{k+1}}{\overset{a_k}{\rightleftarrows}} D_{k+1} \quad (\text{coarsening and dissociation})\\ &\qquad \text{for } k = m, \ldots, L-1,\\ &D_k + D_j \underset{g_{k+j}}{\overset{f_{kj}}{\rightleftarrows}} D_{k+j} \quad (\text{fusion and fission})\\ &\qquad \text{for } 2m \le k + j \le L, \end{aligned} \tag{1}$$

where P denotes a single protein and D_k denotes a droplet consisting of k proteins. m indicates the threshold number of proteins to form a droplet. We model the reactions in (1) with a continuous-time Markov chain, which tracks the copy numbers of each "species" P and D_i. We derive the closed form of the stationary probability distribution of this Markov chain using biochemical reaction network theory. The reaction rate parameters [a_k, b_k, f_{ij}, and g_{i+j} in (3)] are set via first passage time theory of diffusion processes to reflect spatial dimension differences. We then study how these dimensional disparities in diffusion yield differences for LLPS by computing the resulting stationary distribution of (1).

The theoretical study of LLPS spans various fields. In physical chemistry, scientists have investigated LLPS phenomena under thermodynamic theory by measuring energy, showing that energy minimization leads to the demixing of substances and liquid state phase separation.[4,38–40] In addition, theorists used partial differential equation models, such as the Cahn–Hilliard equation,[41] Allen–Cahn equation,[42] and Cahn–Hilliard–Navier–Stokes equation,[43] to analyze and numerically simulate LLPS.[44–49] Machine learning and data-driven methods have also been employed to analyze phase separation.[50] In contrast to previous models that primarily use thermodynamic frameworks such as free energy and chemical potentials to explain LLPS, our model is built from first hitting times of diffusing proteins.

We now briefly summarize our results and their biophysical implications. We first verify that our model reproduces the appropriate phase diagram and phase separation and is consistent with existing thermodynamic models. We then study qualitative differences between 2D-LLPS and 3D-LLPS via the stationary distribution of the reaction network (1). The shape of the stationary distribution is determined by protein characteristics such as the droplet viscosity, the minimum size of droplets, and the hydrodynamic radius of proteins. We first investigate the effect of the droplet viscosity, indicating the strength of the protein–protein interactions. Within a wide range of droplet viscosity values, we find that 2D-LLPS forms large droplets, while proteins are likely to remain without forming in 3D-LLPS. Notably, a higher droplet viscosity is required in 3D than in 2D to increase the droplet size. Next, we find that there exists a range of the minimum droplet size in which 2D- and 3D-LLPS have significantly different probabilities of forming droplets. Finally, we show that when proteins are tethered on a membrane yielding a reduction on the hydrodynamic radius of the protein, less droplets in 2D can be produced compared to a 3D space, but only for a sufficiently large reduction. We present these results using both mathematical analysis and numerical computations.

The stationary distribution thus reveals how diffusion in 2D vs 3D yields differences between 2D-LLPS and 3D-LLPS. Importantly, the stationary distribution is independent of the diffusion coefficient. Therefore, our analysis predicts that prominent qualitative differences between 2D-LLPS and 3D-LLPS stem from fundamental differences in spatial dimension rather than solely from differences in diffusion coefficients. To our knowledge, our study provides the first model of intracellular LLPS using first passage time analysis, chemical reaction network theory, and continuous-time Markov chains.

This paper is organized as follows. We first introduce biochemical reaction networks, one of the key theoretical frameworks of this study, in Sec. II. In that section, we also derive the closed form stationary distribution of the copy numbers of the proteins and the droplets. In Sec. III, we use first passage time theory to set the reaction rates. In Sec. IV, the main results are provided: reproduction of thermodynamic description of LLPS with our model and the qualitative differences of stationary distributions modeling 2D- and 3D-LLPS in terms of viscosity, threshold droplet size, and hydrodynamic radius of proteins. In Sec. V, we provide mathematical analyses of our main results. We conclude in Sec. VI by discussing potential avenues for future work.

II. REACTION NETWORK DESCRIPTION OF LLPS

We develop a stochastic process modeling LLPS based on reaction networks to describe LLPS in both 2D and 3D cellular environments. A reaction network is a graph whose nodes and edges represent complexes and reactions, respectively. For example, in (3), the reaction $P + D_k \to D_{k+1}$ describes the coarsening of the droplet of k proteins by recruiting an additional protein P. The reactant $P + D_k$ is a complex consisting of a single copy of P and a single copy of D_k, and D_{k+1} is the product complex of the reaction.

We use a continuous-time Markov chain to model the stochastic evolution of the copy numbers of species in a reaction network. In particular, let $X(t) = (P(t), D_m(t), \ldots, D_L(t))$ be a continuous-time Markov chain associated with (1). Each coordinate of $X(t)$ gives the copy number of the corresponding species at time t [Fig. 1(c)]. The evolution of X is given by a reaction. For example, if $P + D_m \to D_{m+1}$ fires at t, then $X(t) - X(t-) = (-1, -1, 1, 0, \ldots)$. The reaction to fire and the time for the next reaction are randomly

determined using the reaction intensity $\lambda_{y\to y'}$ for a reaction $y \to y'$ defined as

$$P(X(t+\Delta t) = x + \nu_{y\to y'} \mid X(t) = x) = \lambda_{y\to y'}(x)\Delta t + o(\Delta t) \quad \text{as } \Delta t \to 0+, \tag{2}$$

where $\nu_{y\to y'}$ is the *reaction vector* describing the net change of the reaction $y \to y'$. For example, $\nu_{mP\to D_m} = (-m, 1, 0, 0, \ldots)$. The function $\lambda_{y\to y'}$ provides the rate of the transition given by the reaction $y \to y'$.[23] Hence, these intensities fully characterize X. We now highlight important assumptions for modeling LLPS.

(i) We assume that the timescale of LLPS is faster than protein production and degradation. Hence, we do not consider production and degradation reactions, $\emptyset \to P$ and $P \to \emptyset$.

(ii) We do not consider the reactions $kP \to D_k$ for $k < m$ because we assume that there exists a threshold number, m, of proteins to form a droplet [Fig. 1(b)]. The existence of such a threshold was experimentally and theoretically verified in Ref. 51. The volume fraction of the dense phase under the stationary distribution of $X(t)$, which we derive in (8), can also be used to theoretically support this. We provide more details about this setting in Appendix A 1.

(iii) Proteins inside droplets are expected to have a smaller mobility compared to proteins outside droplets,[9,52] which means that f_{kj} and g_{k+j} are much smaller than the other reaction rates. Hence, to simplify our analysis, we neglect the fusion reactions and the fission reactions $D_j \overset{f_{kj}}{\underset{g_{k+j}}{\rightleftarrows}} D_{k+j}$ (see Appendix A 5 for details on this assumption).

Under these assumptions, the reaction network describing LLPS in this paper is

$$mP \underset{b_m}{\overset{a_1}{\rightleftarrows}} D_m, \quad P + D_k \underset{b_{k+1}}{\overset{a_k}{\rightleftarrows}} D_{k+1} \text{ for } k = m, \ldots, L-1. \tag{3}$$

Remark 1. The reactions in (3) do not result in chemical changes on the proteins or the droplets, although such reactions are often termed "chemical reactions" in mathematical biology or chemical reaction network theory. For example, the birth of an animal can be described with a chemical reaction $A \to 2A$. In the same sense, we also emphasize that the reactions in (3) do not mean protein assembly, which is a chemical process related to but distinct from LLPS. We discuss protein assembly in relation to our modeling in Appendix A 3.

In Sec. IV (a) and Appendix A, we describe how this model is consistent with certain thermodynamic aspects of LLPS. Based on mass-action kinetics, the intensities of the reactions in (3) are defined at $\mathbf{x} = (p, d_m, \ldots, d_L)$ as

$$\begin{aligned} \lambda_{mP\to D_m}(\mathbf{x}) &= a_1 p(p-1)\cdots(p-m+1)\mathbb{1}_{p\geq m}, \\ \lambda_{D_m\to mP}(\mathbf{x}) &= b_m d_m \mathbb{1}_{d_m\geq 1}, \\ \lambda_{P+D_k\to D_{k+1}}(\mathbf{x}) &= a_k p d_k \mathbb{1}_{p\geq 1}\mathbb{1}_{d_k\geq 1}, \end{aligned} \tag{4}$$

and

$$\lambda_{D_{k+1}\to P+D_k}(\mathbf{x}) = b_{k+1} d_{k+1} \mathbb{1}_{d_{k+1}\geq 1}$$

for $k = m, \ldots, L-1$. Here, $\mathbb{1}_A$ denotes the indicator function, which is 1 if the condition A is satisfied and is zero otherwise. For instance,

$$\mathbb{1}_{p\geq m} = \begin{cases} 1 & \text{if } p \geq m, \\ 0, & \text{otherwise.} \end{cases} \tag{5}$$

Abusing notation, for a reaction $y \to y'$, we can regard the complexes y and y' as vectors. For example, the complexes mP and $P + D_m$ can be represented by $(m, 0, \ldots, 0)$ and $(1, 1, 0, \ldots, 0)$, respectively. Then, for $y \to y'$, the reaction vector can be denoted by $y' - y$, which means the net gain of species via the reaction $y \to y'$. The probability distribution $p(\mathbf{x}, t) = P(X(t) = \mathbf{x})$ of $X(t)$ is governed by the *chemical master equation*, a system of ordinary differential equations defined as

$$\begin{aligned} \frac{d}{dt}p(\mathbf{x}, t) &= \lambda_{mP\to D_m}(\mathbf{x} - (-m, 1, 0, \ldots, 0))\, p(\mathbf{x} - (-m, 1, 0, \ldots, 0), t) \\ &\quad + \lambda_{D_m\to mP}(\mathbf{x} - (m, -1, 0, \ldots, 0))\, p(\mathbf{x} - (m, -1, 0, \ldots, 0), t) \\ &\quad + \sum_{k=m}^{L-1} \left(\lambda_{P+D_k\to D_{k+1}}(\mathbf{x} - \nu_k^+)\, p(\mathbf{x} - \nu_k^+, t) \right. \\ &\quad \left. + \lambda_{D_{k+1}\to P+D_k}(\mathbf{x} - \nu_k^-)\, p(\mathbf{x} - \nu_k^-, t) \right) \\ &\quad - \left(\lambda_{mP\to D_m}(\mathbf{x}) + \lambda_{D_m\to mP}(\mathbf{x})\right) p(\mathbf{x}, t) \\ &\quad + \sum_{k=m}^{L-1} \left(\lambda_{P+D_k\to D_{k+1}}(\mathbf{x}) + \lambda_{D_{k+1}\to P+D_k}(\mathbf{x})\right) p(\mathbf{x}, t), \end{aligned} \tag{6}$$

where ν_k^+ and ν_k^- are the reaction vectors associated with $P + D_k \to D_{k+1}$ and $D_{k+1} \to P + D_k$, respectively, for each k.

Remark 2. A well-known reaction network, the so-called Becker–Döring model, has a similar reaction network structure to (3).[53–55] This model is often employed to describe particle aggregation. However, due to the absence of the threshold of the protein concentration, this prior model is limited to describing protein assembly rather than phase separation (see Ref. 2 for the difference between protein assembly and phase separation).

A. Stationary distributions

We analyze the differences between 2D-LLPS and 3D-LLPS using their stationary distributions. The stationary distribution is the limiting distribution of $p(\mathbf{x}, t)$ defined as

$$\lim_{t\to\infty} p(\mathbf{x}, t) = \pi(\mathbf{x}) \quad \text{for each } \mathbf{x}. \tag{7}$$

One advantage of the chemical reaction network description of LLPS is that we can obtain the closed form of π. To do this, we use Theorem 1[56] (see Appendix C).

Using Theorem 1, the stationary distribution of the associated Markov chain for (3) is for each $\mathbf{x} = (p, d_m, \ldots, d_L)$,

$$\pi(\mathbf{x}) = M \frac{1}{p!} \prod_{k=m}^{L} \frac{Q_k^{d_k}}{d_k!} \tag{8}$$

for each state $\mathbf{x}$, where Q_k is

$$Q_k := \begin{cases} \left(\frac{a_1}{b_m}\right) & \text{if } k = m, \\ \left(\frac{a_1 a_m, \cdots a_{k-1}}{b_m b_{m+1} \cdots b_k}\right) & \text{if } m < k \le L. \end{cases} \tag{9}$$

The constant M is the normalizing constant such that

$$M = \left(\sum_{\mathbf{x} \in S_{\mathbf{x}}} \frac{1}{p!} \prod_{k=m}^{L} \frac{Q_k^{d_k}}{d_k!} \right)^{-1}, \tag{10}$$

where $S_{\mathbf{x}}$ is the state space containing $\mathbf{x}$.

One of the advantages of the closed form of the stationary distribution (8) for our model is its ability to generalize the numerical results shown in Sec. IV. Indeed, the threshold number of proteins to form droplets (m) and the size of the largest droplet (L) can vary widely depending on several factors, including the concentration of the proteins, their affinities to each other, and the specific conditions of the system.[57,58] Owing to computational costs, we often use small values of m and L for simulations, since the size and complexity of the state space of the model grow rapidly with these parameters. However, due to the closed form of (8), we show that our main results hold for general m and L (see Propositions 3–4).

III. REACTION RATES

We choose the reaction rates in our model (3) by regarding each protein as a randomly diffusing particle. We consider either a disk (for 2D-LLPS) or a sphere (for 3D-LLPS) surrounding droplet to present a target of particles (proteins) as shown in Fig. 1(d). We view a protein as a circular/spherical object with a *hydrodynamic radius* r that takes into account the hydrodynamic length of the protein or the interaction range of a single protein as shown in Fig. 1(d). Assuming that the volume of a droplet D_k is proportional to the number of proteins k, the radius $r_{k,d}$ of the droplet D_k in d-dimensional space satisfies

$$r_{k,d} = \begin{cases} \alpha r k^{1/2} & \text{if } d = 2, \\ \alpha r k^{1/3} & \text{if } d = 3, \end{cases} \tag{11}$$

for each $k = m, m+1, \ldots, L$. [See Fig. 1(d) for this derivation.] The proportionality constant α may vary by the protein–protein binding affinity and density of the protein aggregation. We simply set $\alpha = 1$ throughout this article.

We assume that the reaction $P + D_k \to D_{k+1}$ fires when a particle (protein) hits the target D_k. Hence, the rates a_k can be defined using first hitting times. Similarly, we define a_1 and b_k by regarding the proteins as diffusing particles.

Throughout this article, $\|v\| = \sqrt{\sum_{i=1}^{K} v_i^2}$ denotes the standard Euclidean norm of a vector $v \in \mathbb{R}^K$. Furthermore, $d = 2$ or 2D and $d = 3$ or 3D indicate two-dimensional LLPS and three-dimensional LLPS, respectively.

A. The initial droplet formation rate, a_1

The main idea for the generalized Smoluchowski framework introduced in Ref. 59 is to consider m independent d-dimensional Brownian particles $B_i(t)$ $(i = 1, 2, \ldots, m)$ with diffusion coefficient D within the spherical or circular system domain $\Omega = \{x : \|x\| \le R\}$ for some $R > 0$. In Ref. 59, probability fluxes were used to determine the rate constant for m particles to be in close proximity. It was also shown that a Markov chain under mass-action kinetics with the generalized Smoluchowski rate can closely approximate the same system modeled with Brownian particles.[59] Note that the shape of the domain is irrelevant when the particle is sufficiently small relative to the domain. Then, the reaction rate a_1 can be set as

$$a_1 = \left[T_m \frac{4\pi^{\alpha_d + 1} r_{m,d}^{2\alpha_d}}{\Gamma(\alpha_d)} \right] / V^{m-1}, \tag{12}$$

where $r_{m,d}$ is as (11), $T_m = D \times \frac{m^{3/2}}{m!} \left(\frac{m-1}{2}\right)^{(3m-5)/2}$, $\alpha_2 = (m-2)$, $\alpha_3 = (3m-5)/2$, Γ is the gamma function, and V is the volume of the system domain [see Ref. 59, Eq. (3.22)]. Note that

$$V = \begin{cases} \pi R^2 & \text{if } d = 2, \\ \frac{4}{3}\pi R^3 & \text{if } d = 3. \end{cases} \tag{13}$$

Then, (11) yields that

$$a_1 = \begin{cases} T_m \left[\frac{4m^{m-2}}{\Gamma(m-2)} \right] \left(\frac{r}{R} \right)^{2m-2} \frac{1}{r^2} & \text{if } d = 2, \\ T_m \left[\left(\frac{3}{4\sqrt{\pi}} \right)^{m-1} \frac{4m^{(3m-5)/3}}{\Gamma((3m-5)/2)} \right] \left(\frac{r}{R} \right)^{3m-3} \frac{1}{r^2} & \text{if } d = 3. \end{cases} \tag{14}$$

Note that $m \ge 3$ throughout this paper.

We now observe from (14) that for any m, the rate of initial droplet formation a_1 in 2D-LLPS is much greater than in 3D-LLPS since $r \ll R$, as long as the 3D diffusion coefficient is not far larger than the 2D diffusion coefficient. That is, the generating time of a droplet in 2D is faster than in 3D [Fig. 1(g)].

Remark 3. The term $m!$ in T_m comes from mass-action kinetics for $mP \to D_m$. The intensity of $mP \to D_m$ under mass-action kinetics is combinatorially defined as it is proportional to $\binom{P}{m} = \frac{P(P-1)\cdots(P-m+1)}{m!}$. Hence, we merge the term $m!$ to a_1.

B. The droplet coarsening rate, a_k, for $m + 1 \le k \le L - 1$

In our LLPS model, droplet coarsening happens when a protein hits the droplet. We thus model the rates of the coarsening reaction $P + D_k \xrightarrow{a_k} D_{k+1}$ using the mean first hitting time for a protein to hit a droplet D_k [Fig. 1(f)]. Hence, we first consider the d-dimensional annular domain,

$$\Omega_{k,d} := \{x \in \mathbb{R}^d : r_{k,d} \le \|x\| \le R\}.$$

As in Sec. III A, an individual protein is described by a Brownian motion $B(t)$ with diffusion coefficient D. Let $\tau_{k,d}$ denote the first hitting time in d-dimensional space,

$$\tau_{k,d} = \inf\{t \ge 0 : \|B(t)\| = r_{k,d}\}. \tag{15}$$

For $k \in \{m, m+1, \ldots, L-1\}$, taking the leading order behavior as $r/R \to 0$ yields[60]

$$\frac{1}{\mathrm{E}[\tau_{k,d}]} \sim a_k = \begin{cases} \dfrac{(2D/R^2)}{\ln(R/r) + \ln k^{-1/2}} & \text{if } d=2, \\ \dfrac{3D}{R^2} k^{1/3} \dfrac{r}{R} & \text{if } d=3. \end{cases} \tag{16}$$

This rate of coarsening can also be obtained as a Smoluchowski reaction rate.[61] Indeed, the Smoluchowski reaction rate for two particles is proportional to the inverse of the mean first hitting time $\mathrm{E}[\tau_{k,d}]$, implying consistency between a_k and the Smoluchowski rate.[62,63]

Remark 4. In the formulation of $\tau_{k,d}$ in (15), the circular (spherical) target is assumed to be centered at the origin. However, by the Markovianity of $B(t)$, the initial positions of $B(t)$ and the target D_k are negligible for the derivation of (16) provided that the target is sufficiently small relative to the size of the domain Ω. In this vein, we need not assume that the domain Ω is either circular or spherical.

C. The dissociation rate, b_k

We now set the rate of the dissociation reactions $D_{k+1} \xrightarrow{b_k} P + D_k$. One of the key features of LLPS is that the droplets are liquid. Hence, we determine b_k for the first time when a diffusing protein inside a droplet hits the boundary of the droplet [Fig. 1(f)].

We anticipate that proteins within droplets exhibit significantly slower diffusion coefficients compared to those outside droplets due to interactions with other proteins within the confined environment.[9,52] We simply incorporate this effect by a constant V. This constant will be set by considering various factors including viscosity, valency, the binding affinity of proteins, and surface tension.[64–67] We will simply call V the viscosity constant. In particular, we use V as a scaling parameter for the diffusion coefficient of the protein within a droplet as $\tilde{D} = \frac{D}{V}$.

The valency refers to the number of binding sites a protein has, allowing it to interact with other proteins. An increased valency can reduce the threshold concentration for phase separation.[2] This may imply that there is less dissociation with higher valency, which we can model by setting V as an increasing function of valency. The binding affinity is the strength of protein–protein interactions. Higher binding affinity reduces the dynamic rearrangements of molecules within phase-separated droplets.[68,69] Hence, the diffusion coefficient $\tilde{D}$ decreases with the binding affinity.[65,67] Existing studies indicate that droplets with higher stability have higher surface tension,[70] and thus, we can suppose that the viscosity constant increases with surface tension. Summarizing, an increase in any of these factors increases the viscosity constant V.

We now consider for the first time a Brownian particle to exit a disk (or a sphere) of radius $r_{k,d}$, starting from the center. For each $k \in \{m, m+1, \ldots, L\}$, let

$$\tilde{\tau}_{k,d} = \inf\{t \geq 0 : \|B(t)\| \geq r_{k,d}\},$$

where $B(t)$ is a Brownian motion in $\mathbb{R}^d$ with the diffusion coefficient $\tilde{D}$, and $r_{k,d}$ is defined as in (11). The mean first passage time $\tilde{\tau}_{k,d}$ is[71]

$$\frac{1}{\mathrm{E}[\tilde{\tau}_{k,d}]} = \begin{cases} \dfrac{4\tilde{D}}{(r_{k,d})^2} & \text{if } d=2, \\ \dfrac{6\tilde{D}}{(r_{k,d})^2} & \text{if } d=3. \end{cases} \tag{17}$$

Since each D_k contains k proteins, we multiply the inverse of the mean first passage time by k to set b_k. That is,

$$\frac{k}{\mathrm{E}[\tilde{\tau}_{k,d}]} = b_k = \begin{cases} \dfrac{4k\tilde{D}}{(r_{k,d})^2} = \dfrac{4D}{Vr^2} & \text{if } d=2, \\ \dfrac{6k\tilde{D}}{(r_{k,d})^2} = \dfrac{6Dk^{1/3}}{Vr^2} & \text{if } d=3. \end{cases} \tag{18}$$

Note that the dissociation rate constant b_k does not depend on k in 2D, while it does in 3D.

Remark 5. The binding affinity affects α in (11), which scales the droplet size based on protein–protein bonding. It is natural to choose α as a decreasing function of the binding affinity. Although we set the reaction proximity for $mP \to D_m$ and the hydrodynamics radius of D_k to be the same when $\alpha = 1$, they should be treated differently when $\alpha \neq 1$. Recall that for simplicity, we set $\alpha = 1$ in this paper.

D. Analysis of rate constants

To summarize, the reaction rates are given by

$$a_1 t_0 = \begin{cases} \gamma_2 \varepsilon^{2\alpha_2} & \text{in 2D}, \\ \gamma_3 \varepsilon^{2\alpha_3} & \text{in 3D}, \end{cases} \tag{19}$$

$$a_k t_0 = \begin{cases} -2/\ln \varepsilon & \text{in 2D for } k \geq m+1, \\ 3\varepsilon k^{1/3} & \text{in 3D for } k \geq m+1, \end{cases} \tag{20}$$

$$b_k t_0 = \begin{cases} 4\dfrac{1}{V}\varepsilon^{-2} & \text{in 2D}, \\ 6\dfrac{1}{V}\varepsilon^{-2}k^{1/3} & \text{in 3D}, \end{cases} \tag{21}$$

where $t_0 = R^2/D$ denotes the diffusion timescale, $\varepsilon = r/R \ll 1$ measures the length scale of protein interactions to the size of the confining spatial domain, $V \gg 1$ measures how protein diffusion slows in droplets, $\alpha_2 = m-2$, $\alpha_3 = (3m-5)/2$, and

$$\gamma_d = \begin{cases} m^{3/2}\left(\dfrac{m-1}{2}\right)^{\frac{3m-5}{2}}\left[\dfrac{4m^{m-2}}{\Gamma(m-2)}\right] & \text{if } d=2, \\ m^{3/2}\left(\dfrac{m-1}{2}\right)^{\frac{3m-5}{2}}\left[\left(\dfrac{3\sqrt{3}}{4\pi}\right)^{m-1}\dfrac{4m^{(3m-5)/3}}{\Gamma((3m-5)/2)}\right] & \text{if } d=3. \end{cases} \tag{22}$$

Note that we have ignored the higher order k dependence in γ_d in 2D since we assume that $k \ll 1$.

There are several noteworthy features of (19)–(21). First,

$$a_1^{3D}/a_1^{2D} = O(\varepsilon^{m-1}) \quad \text{as} \varepsilon \to 0. \tag{23}$$

Hence, the formation rate of an initial droplet consisting of m proteins is much faster in 2D than in 3D. Second, for $m > 1$,

$$a_k^{3D}/a_k^{2D} = O(\varepsilon \ln \varepsilon) \quad \text{as} \varepsilon \to 0. \tag{24}$$

Hence, droplet coarsening is also faster in 2D than in 3D, although the difference between 2D and 3D is not as pronounced as it is for the initial droplet formation rates a_1^{2D} and a_1^{3D}. Third,

$$b_k^{3D}/b_k^{2D} = O(1) \quad \text{as} \varepsilon \to 0. \tag{25}$$

Hence, droplet dissociation in 2D and 3D occurs at similar rates. Finally, the rate of droplet coarsening and dissociation grows with droplet size k in 3D, but these rates are independent of the droplet size k in 2D (to leading order for $\varepsilon \ll 1$). From this analysis, we can expect that 2D is more favorable for phase separation than 3D as schematically described in Fig. 2(a). The main results of this paper, which are given in Sec. IV, depend on this analysis [see Fig. 2(b) for a schematic summary].

IV. RESULTS

Here, we provide four main results for a qualitative comparison between 2D-LLPS and 3D-LLPS. We use plots of the stationary distribution π and stochastic simulations to show our results and validate the analyses in Sec. III D. In Sec. V, we provide proofs verifying our results. Without loss of generality, we use a unit radius of the system domain, $R = 1$, for all the following simulations [except for Fig. 3(c)].

A. Reproduction of LLPS

Here, we show the consistency of our model with certain aspects of thermodynamics. Thermodynamic analysis validates that when the total concentration of the system, ϕ^*, is the system admits the coexistence of dilute phases of concentration ϕ_1 and dense phases of concentration ϕ_2 rather than a single phase of concentration ϕ^* [Fig. 3(a)]. This is due to the concave region of the free energy function that implies that the convex combination of the free energies at ϕ_1 and ϕ_2 is less than the free energy at the concentration ϕ^*. That is, $sF(\phi_1) + (1-s)F(\phi_2) < F(\phi^*)$ for s such that $s\phi_1 + (1-s)\phi_2 = \phi^*$ (for more details, see Ref. 4). This induces phase separation, and the phase diagram is derived as shown in Fig. 3(b). This phase separation and the phase diagram can be reproduced with samples of our Markov chain $X(t)$ in (3) modeled with the reaction rates defined in Sec. III.

We first visualize samples of $X(t)$ in 2D to show how our model can describe phase separation. Once an initial condition $X(0) = (P_{tot}, 0, 0, \ldots)$ is fixed, where P_{tot} is the initial protein count, we sample a single trajectory in time $X(t) = (P(t), D_m(t), \ldots, D(t))$ using the statistically exact Gillespie algorithm.[73] The plot of $X(t)$

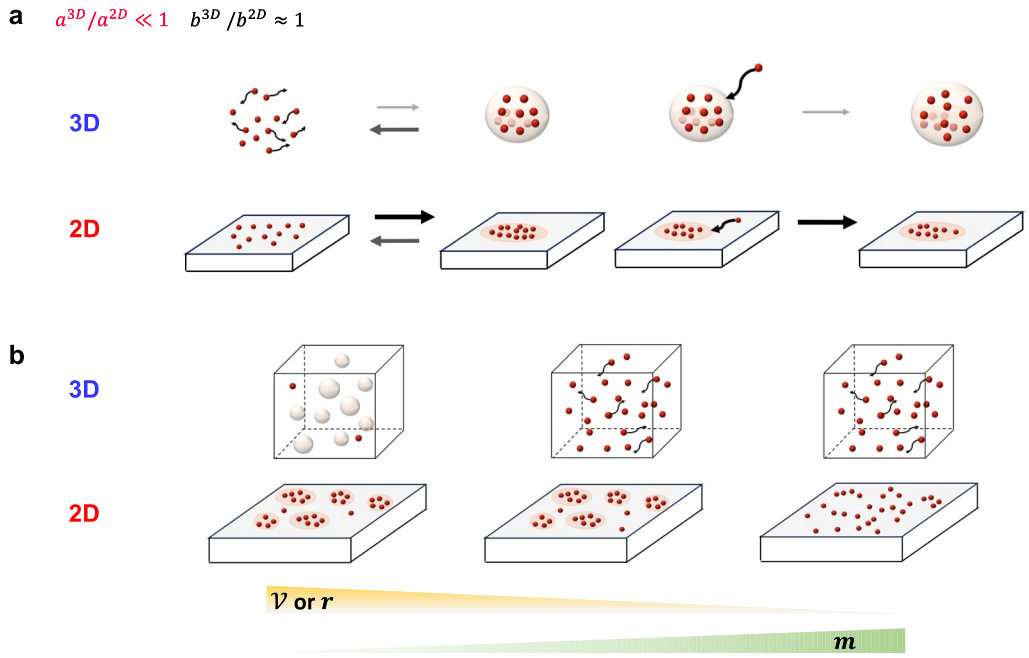

FIG. 2. Summary of the analysis of the rates. (a) Under identical settings, due to the differences in a_1 and a_k between 2D and 3D, droplet formation and coarsening occur more quickly in 2D than in 3D. (b) We schematically summarize the main results of this paper. The higher the viscosity (or the hydrodynamic radius), both 2D and 3D have more droplets. However, 2D and 3D have different responses to changes in $\mathcal{V}$ or r. Similarly, while both have fewer droplets with a higher m, they have different responses to changes in m.

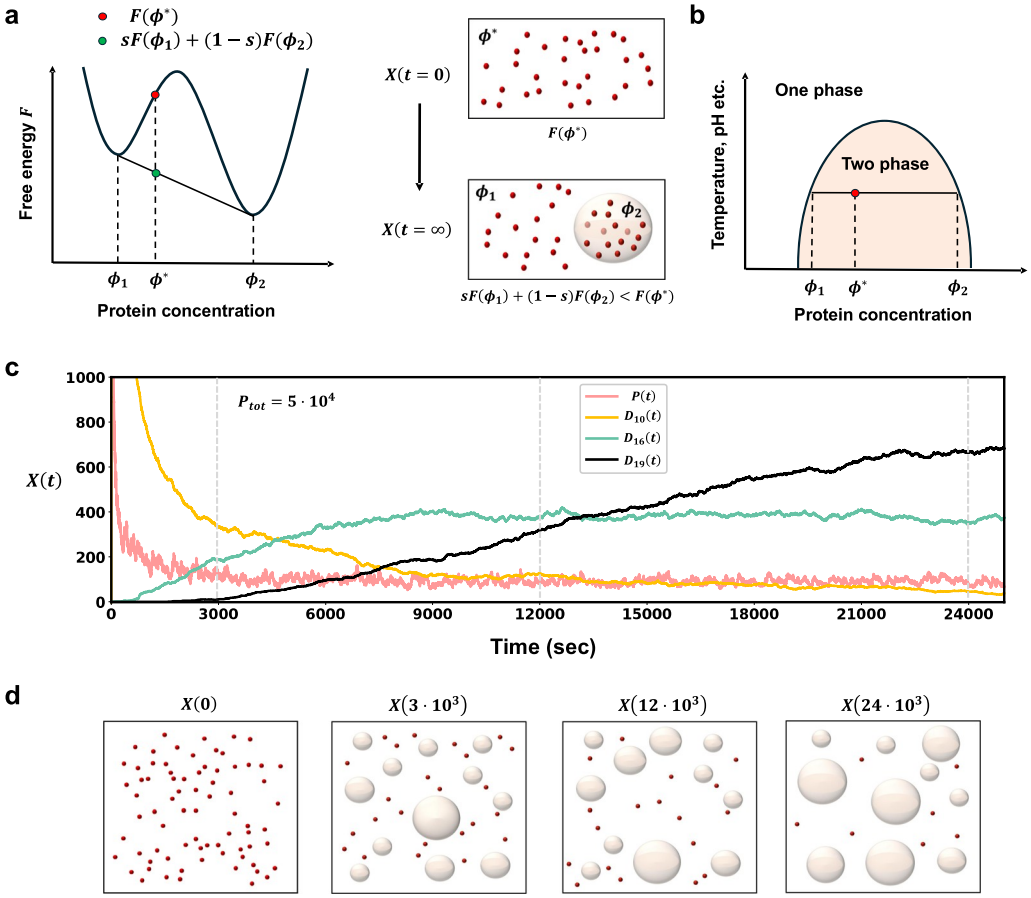

FIG. 3. Reproduce of phase separation. (a) and (b) Free energy explains phase separation and the phase diagram. (c) $X(t) = (P(t), D_m(t), \cdots, D_L(t))$, a time trajectory of $X(t)$ in 2D, shows droplet coarsening and Ostwald ripening. (d) Cartoons of the snapshots of $X(t)$ at four time points.

in Fig. 3(c) (with realistic parameters,[14] see Appendix B) shows the coarsening of the droplets as time passes. Notably, the number of smaller droplets decreases, while the number of bigger droplets increases. Hence, these plots also visualize Ostwald ripening as individual proteins dissociate from a smaller droplet and join a bigger droplet (see Appendix A 2 for more details). Then, we display the sampled state at four time points $t = (0, 3 \cdot 10^3, 12 \cdot 10^3, \text{and } 24 \cdot 10^3)$ by randomly distributing the proteins and the droplets over the space, where the counts of the proteins and droplets are given by $X(t)$ [Fig. 3(d)].

Now, by computing the volume fraction of the dense phase (droplets) and the dilute phase (outside droplets), we reproduce the phase diagram. Let $V_{k,d}$ be the volume of D_k, the droplet of size k. Then,

$$V_{k,d} = \begin{cases} \pi r_{k,d}^2 = \pi r^2 k & \text{if } d = 2, \\ \frac{4}{3}\pi r_{k,d}^3 = \frac{4}{3}\pi r^3 k & \text{if } d = 3. \end{cases} \tag{26}$$

Both the number of proteins in D_k and the volume of D_k grow linearly in k. Hence, the concentration of the proteins inside the droplet D_k is the same for each k, which is consistent with the previous analyses of LLPS.[14]

Let $\mathrm{E}_\pi(P)$ [respectively $\mathrm{E}_\pi(D_k)$] denote the expected number of proteins in the dilute phase (respectively, the droplet of size k) with respect to π in (8). Define the average volume ratio of the droplets to the system size V as

$$\rho := \frac{\sum_{k=m}^{L} V_{k,d} \mathrm{E}_\pi(D_k)}{V} = \begin{cases} \frac{\pi r^2 (P_{tot} - \mathrm{E}_\pi(P))}{V} & \text{if } d = 2, \\ \frac{\frac{4}{3}\pi r^3 (P_{tot} - \mathrm{E}_\pi(P))}{V} & \text{if } d = 3, \end{cases} \tag{27}$$

where we used the conservation of the total protein counts such that

$$P_{tot} := P(t) + \sum_{k=m}^{L} k D_k(t) \quad \text{for each time } t. \tag{28}$$

The ρ in (27) can determine whether the system has either a single phase or two phases. We assume that the system has two phases if $\rho \in (\rho_1, \rho_2]$ for some $\rho_1 < \rho_2$ and has a single phase otherwise. That is, if droplets and proteins coexist with the volume fraction falling in the range, the system has two phases. Furthermore, since the viscosity of liquid droplets and the hydrodynamic radius are specific functions of thermodynamic temperature $T + 273$, which is measured in Kelvin, we define V as a linear function of $e^{1/(T+273)}$ and r as a linear function of $T + 273$, as referenced in the literature[73,74] (a full description of V and r as a function of T is given in Appendix B). In this setting, we regard ρ as a function of the total protein count P_{tot} and the temperature T.

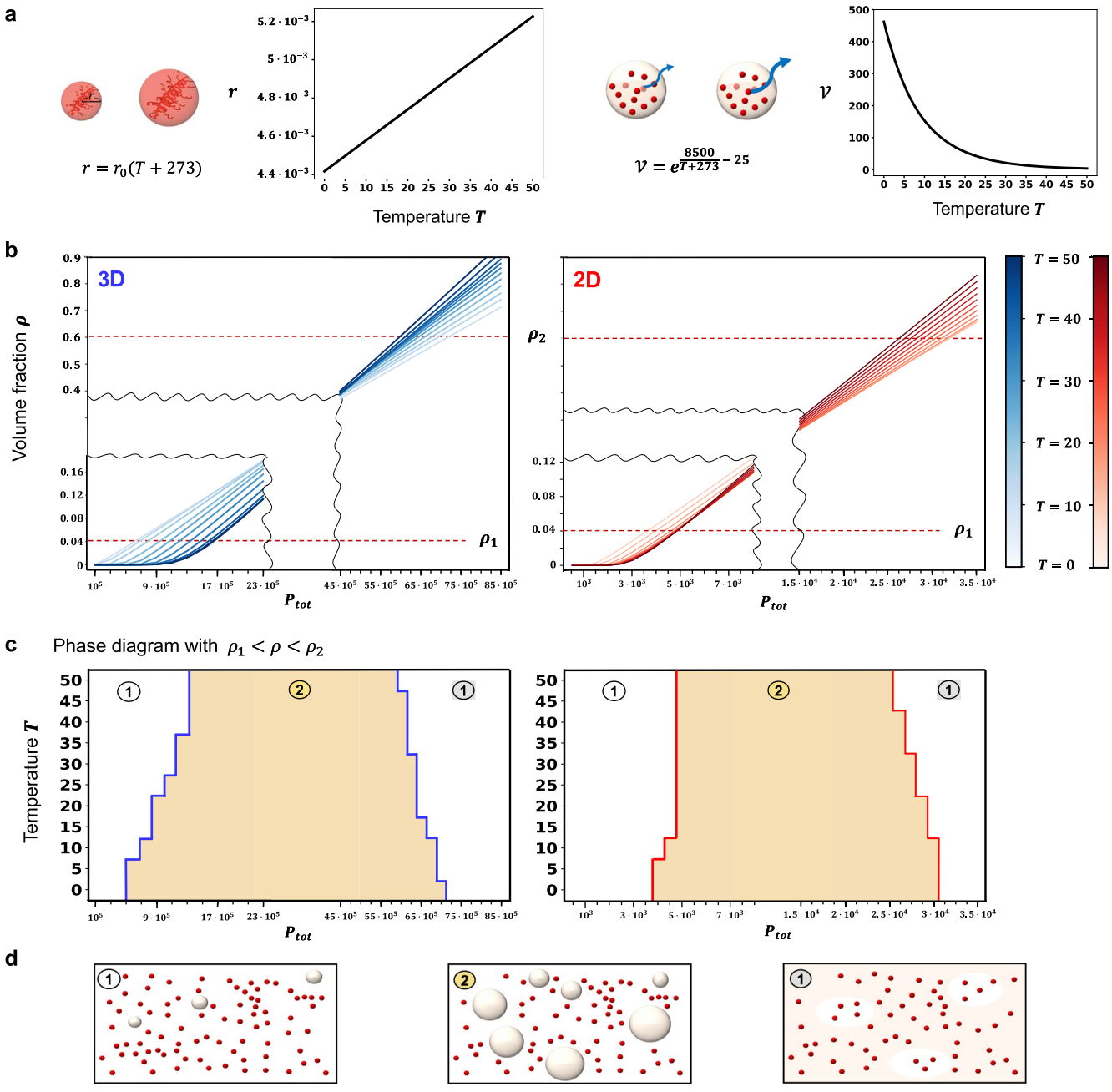

FIG. 4. Reproduction of the phase diagram (a) Effect of temperature on the hydrodynamic radius r and viscosity V with the graphs. (b) The volume fraction (27) as a function of P_{tot} in 2D and 3D. ρ_1 and ρ_2 are the criteria for phase separation. (c) Phase diagrams in 2D and 3D. For example, a system at ① and ② will have a single phase and two phases, respectively, which are schematically illustrated in (d).

To compute the volume fraction using ρ, as described in (8), the state space has to be identified. However, when the initial number of proteins is high, the state space is too large to search numerically. Therefore, we sample $2 \cdot 10^4$ time trajectories, using the Gillespie algorithm[75] for 2D with up to $3 \cdot 10^4$ reactions and the tau-leaping algorithm[76] for 3D with up to $3.5 \cdot 10^4$ reactions. Then, we empirically compute ρ using the samples. The supplementary plots show that the samples with $3 \cdot 10^4$ reactions in 2D and $3.5 \cdot 10^4$ reactions in 3D closely approximate the stationary state of the system in 2D and 3D, respectively (Fig. 9).

Figure 4(b) shows the graph of ρ as a function of P_{tot} with different values of temperature T (Celsius). With this ρ, the phase diagram was obtained from our model with $b_1 = 4 \cdot 10^{-2}$ and $\rho_2 = 0.6$, and it turns out to display the well-known concave curve [Fig. 4(c)].

Remark 6. The plateau of ρ, which appears for small values of P_{tot}, implies that droplets are not formed when the total concentration P_{tot}/V is small. Hence, our model also reproduces the threshold protein concentration for phase separation.

Remark 7. While the threshold volume fractions $4 \cdot 10^{-2}$ and 0.6 used to define the two phases were chosen somewhat arbitrarily in this paper, these values can be justified using existing theory. Indeed, the threshold protein concentrations of the system for phase separation are given by the free energy analysis,[4] which is displayed in Fig. 3. Hence, we can determine ρ_1 and ρ_2 as the volume fractions of the dense phases at the threshold protein concentrations, namely ϕ_1 and ϕ_2 as in Fig. 3(a). Nonetheless, we chose them arbitrarily because for any small values of ρ_1 and for any large values of ρ_2, we will obtain the same concave shape of the phase diagram due to the trends of the volume fraction in Fig. 4(c). Hence, we chose relatively small ρ_2 to avoid highly intensive computations, which is out of the scope of this paper.

Remark 8. Note that Case[19] mentioned that 2D spaces, such as cell membranes, shift the phase diagram to the left, promoting nucleation. Our model can also reproduce such a shift of the phase diagram in 2D-LLPS [Fig. 4(c)].

B. Higher viscosity is required for LLPS in 3D

Here, we show that a higher viscosity is necessary for droplet formation in 3D than in 2D by showing how the viscosity constant V alters the shape of the stationary distributions of 2D-LLPS and 3D-LLPS. To visualize the stationary distributions, we set the initial protein count $P_{tot} = L$ and $2m > L$ so that the state space S of the Markov chain $X(t)$ is

$$S = \{(L, 0, \ldots), (L-m, 1, 0, \ldots), \ldots, (L-m-1, 0, 1, 0, \ldots), \ldots, (0, 0, \ldots, 1)\}, \tag{29}$$

and hence, it can be linearly aligned. We denote these states by

$$\begin{aligned} \mathbf{x}_0 &= (L, 0, 0, \ldots), \\ \mathbf{x}_m &= (L-m, 1, 0, \ldots), \\ \mathbf{x}_{m+1} &= (L-m-1, 0, 1, 0, \ldots), \\ &\vdots \\ \mathbf{x}_L &= (0, 0, 0, \ldots, 1). \end{aligned} \tag{30}$$

We are interested in finding a range of V for which the stationary distribution has a peak at a two-phase state $\mathbf{x}_k$ for some $k \geq m$, where a droplet is formed [Fig. 5(a)]. To do that, we find B_k's such that

$$B_k \leq V < B_{k-1} \quad \text{if and only if} \quad \pi(\mathbf{x}_0) \leq \pi(\mathbf{x}_j) \tag{31}$$

for any $k \leq j \leq L$. Using the closed forms of B_k for both 2D-LLPS and 3D-LLPS, it turns out that a higher V is required for π to have a peak at $\mathbf{x}_k$ for some k in 3D than in 2D [Fig. 5(a)]. As mentioned in Sec. III D, this result is not surprising because the reaction rates a_1 and a_k are faster in 2D, while b_k are comparable in 2D and 3D [Fig. 1(g)].

The closed form of π leads to other interesting analyses about the relation between V and the droplet size distribution. For example, we investigated the range of V for which π has a local maximum at the state $\mathbf{x}_k$ for $m \leq k \leq L$ [Figs. 5(b) and 5(c)]. Let G_k denote the viscosity constant such that

$$G_{k-1} \leq V \leq G_k \quad \text{if and only if} \quad \pi(\mathbf{x}_j) \leq \pi(\mathbf{x}_k) \tag{32}$$

for all $m \leq j \leq L$. 3D-LLPS also required a higher V to have a local maximum at $\mathbf{x}_k$ for some $k \geq m$ than 2D-LLPS [Fig. 5(c)]. G_k can also be related to an important experimentally observed phenomenon, droplet arrest (the growth of small or mid-size of droplets is paused).[18] Precise calculations about B_k and G_k are given in Sec. V A.

The same trend holds for general state spaces with larger P_{tot}. For example, with $P_{tot} = 200$, the selection of marginal stationary distributions for the counts of proteins $P(t)$ and the count of the largest droplet $D(t)$ shows that a smaller number of largest droplets are produced in 3D than in 2D [Fig. 5(d)].

C. For large thresholds, droplets can be formed in 2D but not in 3D

It has been claimed that membranes reduce the threshold concentration for phase separation.[13,14,19] Snead *et al.*[14] showed that anchoring proteins onto membranes may induce a shift of the threshold concentration for phase separation compared to the threshold of 3D LLPS. Motivated by these experimental findings, in this section, we study the effect of m (the threshold number of proteins for forming droplets) on LLPS. By varying m, we measure the probability of the state where droplets are formed. Using identical parameters for 2D-LLPS and 3D-LLPS, we identify a range of m for which the droplet formation probability is (i) nearly one in 2D and (ii) nearly zero for 3D. We prove this mathematically in Sec. V B.

Let $\mathbf{x}_0 = (P_{tot}, 0, \ldots)$, i.e., the state without droplets. We use the probability $1 - \pi(\mathbf{x}_0)$ as a function of m to measure the probability that proteins form droplets. For large m (respectively, small m), the probability $1 - \pi(\mathbf{x}_0)$ is nearly 0 (respectively, 1) for both 2D-LLPS and 3D-LLPS. Interestingly, for m in an intermediate range, $1 - \pi(\mathbf{x}_0)$ in 2D can be much greater than in 3D (Fig. 6). We prove the existence of such a range m in Sec. V B. This difference mainly arises from the rate constant a_1 as we highlight in Sec. III D. In 2D, m copies of proteins closely gather more frequently than in 3D. This result is consistent with the claim of the

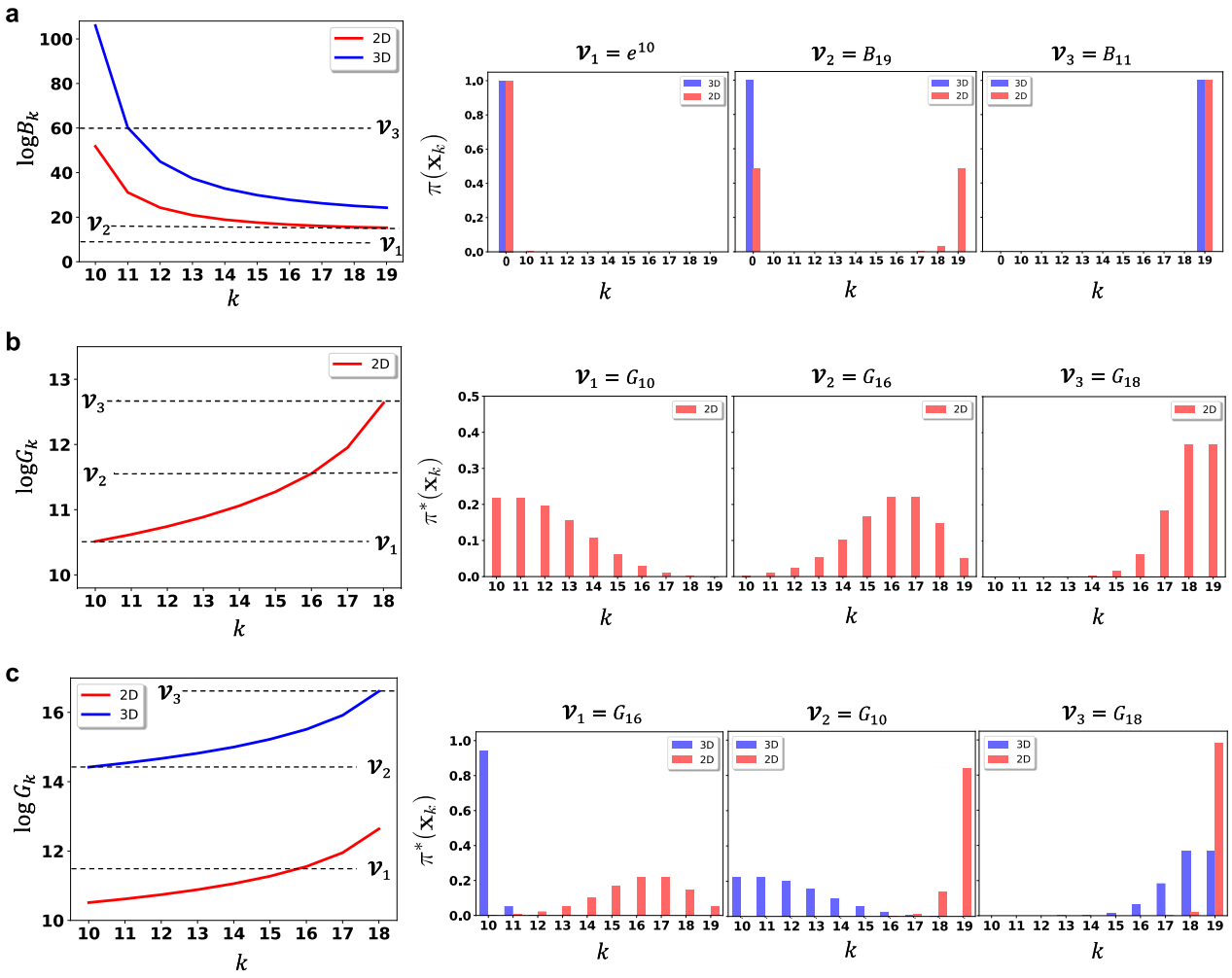

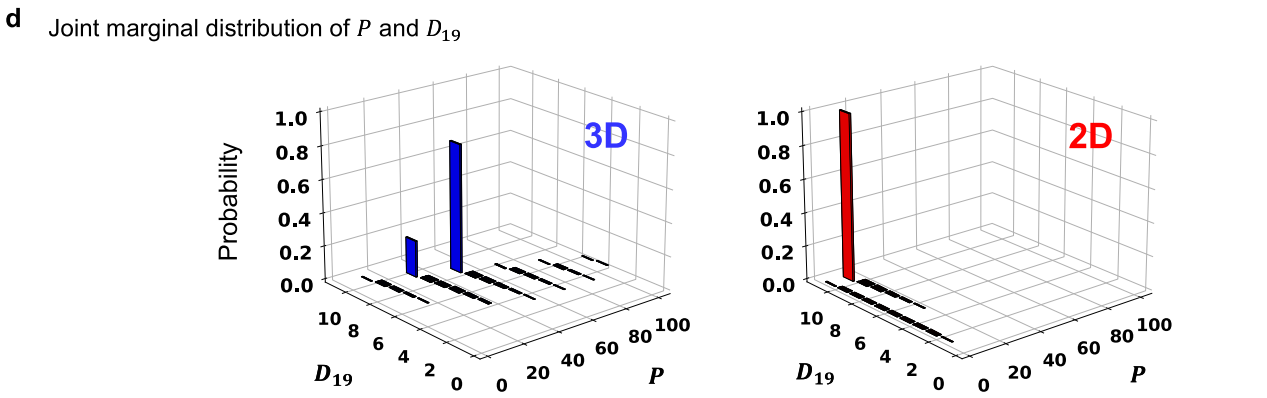

FIG. 5. Effect of V in droplet formation. (a)–(c) The log-scaled graph of B_k and G_k defined as (31) and (32), respectively (left). The stationary distributions of X with $(m, L) = (10, 19)$ and $P_{tot} = L$ show the different probabilities of droplet formation and local maxima in 2D and 3D for certain values of V_i's (right). For (b) and (c), for clearer visualization, we used $\pi^*(\mathbf{x}_k) = \pi(\mathbf{x}_k | P(0) \neq L)$, the stationary distribution conditioned on states consisting of at least one droplet. (d) The joint marginal stationary distributions of P and D_{19} with $P_{tot} = 200$.

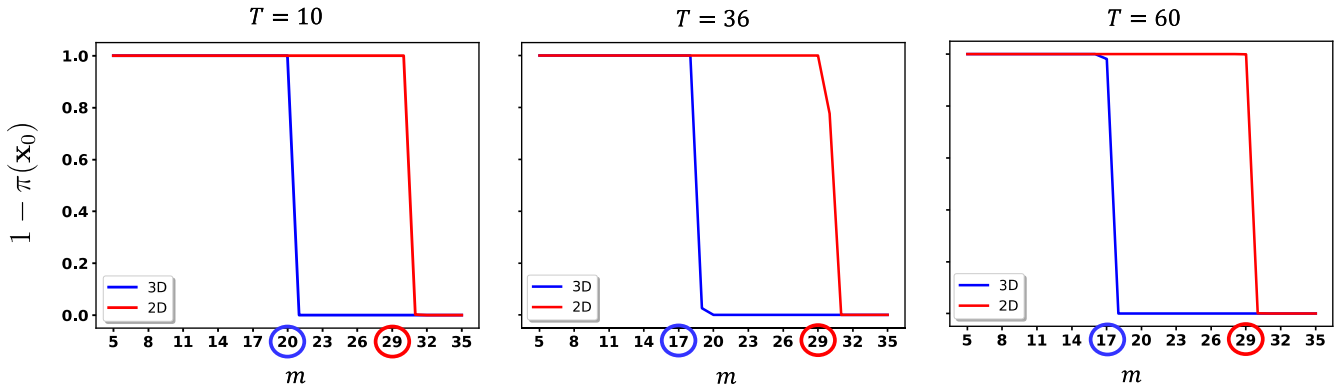

FIG. 6. Effects of m. The plots of the probabilities of droplet formation $[1-\pi(\mathbf{x}_0)]$ as a function of the threshold m with three different choices of temperature T. For both 2D and 3D, there are critical m (indicated with circles) where the probabilities dramatically drop.

previous experimental study[44] that membrane recruitment enhances if and only if the local protein concentration. Thus, we can interpret membrane recruitment as a way for cells to efficiently facilitate the formation of biomolecular condensates at lower costs.[43]

Furthermore, Fig. 6 shows that the droplet formation probability $1-\pi(\mathbf{x}_0)$ decreases dramatically around certain values of m (indicated by circles) in both 2D and 3D. This indicates the sensitivity of droplet formation to the minimum number of proteins or nucleation barriers.[51]

D. Reduction in the hydrodynamic radius in 2D may not be significant

In Sec. III D, we analyzed how the coarsening rate a_1 and the droplet formation rate a_k are greater in 2D than in 3D. This yields the key difference that 2D-LLPS tends to have more droplets than 3D-LLPS. However, by examining the dependence of a_1 on r (14), it can be predicted that anchoring a protein to a membrane surface can reduce the hydrodynamic radius [Fig. 7(a)]. This reduction, in turn, may inhibit droplet formation in 2D. In this section, despite the reduction in r in 2D, the probability of droplet formation is still higher in 2D than in 3D as long as the change in the hydrodynamic radius is not too large. We further analytically quantify the ratio between the hydrodynamic radii in 2D and 3D at which the probability of droplet formation in 3D becomes larger than that in 2D.

Under the same setting of the state space (29), we first display the stationary distributions with different values of r. We denote by r^{2D} and r^{3D} the hydrodynamic radius of a protein in 2D and 3D, respectively. We fix $r^{2D}=0.005$ for 2D-LLPS and set r_i^{3D} for 3D-LLPS as $r_1^{3D}=2r^{2D}$, $r_2^{3D}=5r^{2D}$, and $r_3^{3D}=5.5r^{2D}$. Interestingly, even though $r^{2D}<r_1^{3D}<r_2^{3D}$, the probability of droplet formation, $1-\pi(\mathbf{x}_0)$, remains higher in 2D than in 3D for r_1^{3D} and r_2^{3D} [Fig. 7(b), left and middle]. For r_3^{3D}, 2D and 3D have similar $1-\pi(\mathbf{x}_0)$ [Fig. 7(b), right]. Using the relation

$$F(H):=\log\left(\frac{\sum_{k=m}^{L}\pi^{3D}(\mathbf{x}_k)/\pi^{3D}(\mathbf{x}_0)}{\sum_{k=m}^{L}\pi^{2D}(\mathbf{x}_k)/\pi^{2D}(\mathbf{x}_0)}\right)>0 \tag{33}$$

$$1-\pi^{3D}(\mathbf{x}_0)>1-\pi^{2D}(\mathbf{x}_0), \tag{34}$$

we further see the fold changes of these probabilities by varying H such that $r^{3D}=Hr^{2D}$, where π^{2D} and π^{3D} denote the stationary distributions of $X(t)$ associated with 2D-LLPS and 3D-LLPS, respectively. The plot in Fig. 7(c) (left panel) shows that we can find the critical value of $H=H_0$ such that $F(H_0)=0$, meaning that $1-\pi^{3D}(\mathbf{x}_0)>1-\pi^{2D}(\mathbf{x}_0)$ if and only if $H>H_0$. Using the closed form of π in (8), we can also derive a closed form of H_k's such that for each $k\geq m$,

$$\frac{\pi^{3D}(\mathbf{x}_k)/\pi^{3D}(\mathbf{x}_0)}{\pi^{2D}(\mathbf{x}_k)/\pi^{2D}(\mathbf{x}_0)}\geq 1 \quad \text{if and only if} \quad H\geq H_k. \tag{35}$$

These H_k's guarantee a greater probability of droplet formation in 3D because $F(H)>0$ if $H\geq H_k$ for all k by (33). On top of this, H_k turns out decreasing in k [Fig. 7(c), right]. Hence, we have

$$1-\pi^{3D}(\mathbf{x}_0)>1-\pi^{2D}(\mathbf{x}_0) \quad \text{if} \quad H\geq H_m. \tag{36}$$

See Sec. IV D for the derivation of the closed form of H_k.

V. MATHEMATICAL ANALYSIS

Here, we validate all the results shown in Secs. IV B–IV D using the stationary distributions (8) of the stochastic model for LLPS. Let $S_{\mathbf{x}}$ denote the closed communication class containing the initial state $\mathbf{x}$. We first provide the closed form of Q shown in (9), which will be used for the analysis of the main results. By using the closed form of a_1, a_k, and b_k defined in Secs. III A–III C, we have that for $m\leq k\leq L$,

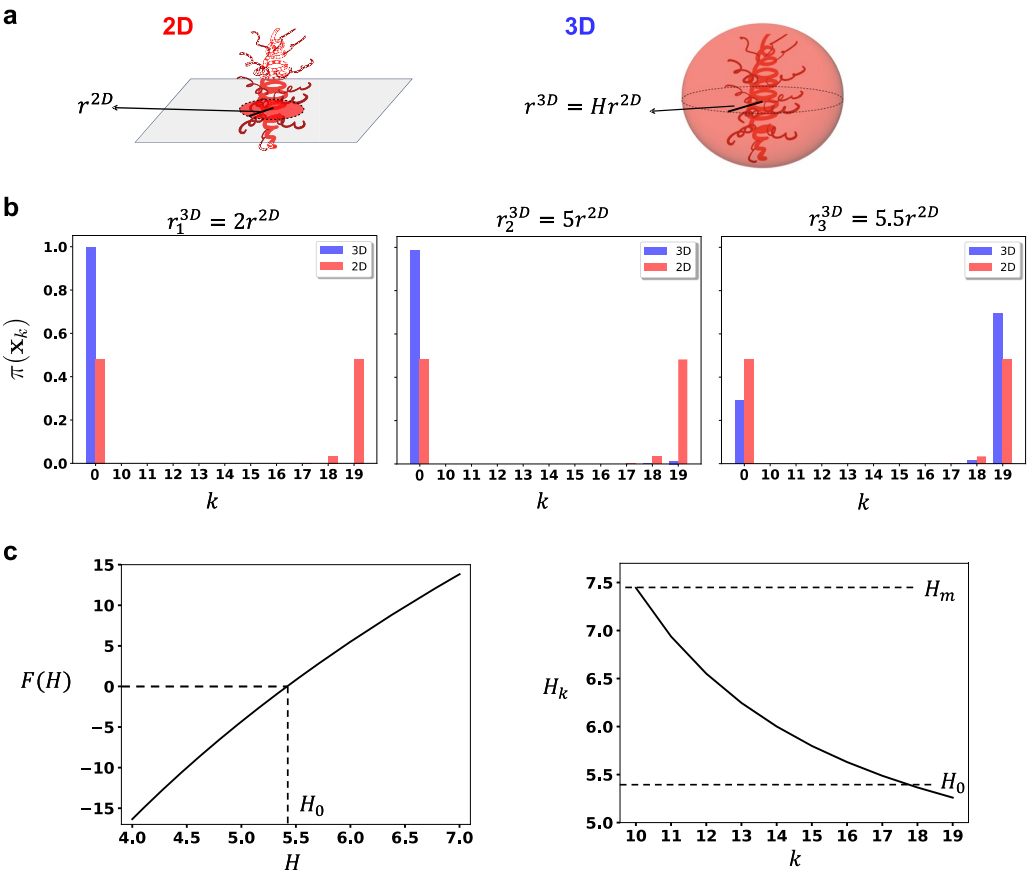

FIG. 7. Effect of r. (a) The hydrodynamic radii of a protein in 2D and 3D spaces. (b) Stationary distributions with a fixed value of r in 2D and with different values of r in 3D. (c) (Left) The plot of $F(H)$ in (33) as a function of the ratio $H = r^{3D}/r^{2D}$ between the hydrodynamic radii. H_0 is the critical value such as $1 - \mathcal{H}^{3D}(\mathbf{x}_0) > 1 - \mathcal{H}^{2D}(\mathbf{x}_0)$ if and only if $H > H_0$. (Right) H_k in (35) is decreasing in k.

$$Q_k := \begin{cases} \dfrac{T_m}{D}\left[\dfrac{m^{m-2}}{\Gamma(m-2)}\right]\dfrac{V^{k-m+1}}{[y^{2k-2}\prod_{s=m}^{k-1}\ln(y^2/s)]} & \text{if } d=2, \\ \dfrac{T_m}{D}\left[\left(\dfrac{3}{4}\right)^{m-1}\sqrt{\pi}^{(m-1)}\dfrac{2m^{(3m-4)/3}}{3\Gamma((3m-5)/2)}\right]\dfrac{V^{k-m+1}}{y^{3k-3}}\left(\dfrac{m^{1/3}}{k^{1/3}2^{k-m}}\right) & \text{if } d=3, \end{cases} \tag{37}$$

where $y = 1/r$, in which r is the hydrodynamic radius of the protein, and T_m is defined in Sec. III A. D represents the diffusion coefficient of a single protein. We also adopt the convention that $\prod_{s=m}^{m-1} u_s = 1$ for any sequence u_s. We further assume that the radius of the domain $R = 1$ with sufficiently small r such that $1/r \ll 1$ and a fixed temperature T.

A. Theoretical validation for Sec. IV B

We demonstrate how the values of Q_k vary with the viscosity constant V. For simplicity, we choose the number of initial proteins $P_{tot} = L$ and $L = 2m - 1$ for a fixed threshold number m of proteins for forming droplets. In this setting, the state space is as (29), and we use the same notations for the states in this section.

We first determine a range of viscosity with which the LLPS model has two modes in the stationary distribution.

Proposition 1. Suppose that $m \geq 5$, $P_{tot} = L$, and $L = 2m-1$ in (3). Then, there exists $\{B_k\}_{m \leq k \leq L}$ such that

$$B_k \leq V \quad \text{if and only if} \quad \pi(\mathbf{x}_0) \leq \pi(\mathbf{x}_k), \tag{38}$$

is equivalent to $B_k \leq V$, where

$$B_k = \begin{cases} \left[\frac{D}{T_m} \frac{(L-k)!}{L!} \left\{ \frac{\Gamma(m-2)}{m^{m-2}} \right\} y^{2k-2} \prod_{s=m}^{k-1} \ln(y^2/s) \right]^{1/(k-m+1)} & \text{if } d=2, \\ \left[\frac{D}{T_m} \frac{(L-k)!}{L!} \left\{ \left(\frac{4}{3}\right)^{m-1} \left(\frac{k^{1/3} 2^{k-m}}{m^{1/3}} \right) \sqrt{\frac{3\Gamma((3m-5)/2)}{\pi^{(m-1)}}} \frac{1}{2m^{(3m-4)/3}} \right\} y^{3k-3} \right]^{1/(k-m+1)} & \text{if } d=3. \end{cases} \tag{40}$$

Now, we turn to show that B_k is a decreasing sequence in 2D.

Note that for each $m \leq k < L$,

$$\log B_k - \log B_{k+1} = C + \frac{2m-4}{(k-m+1)(k-m+2)} \log y + \sum_{s=m}^{k-1} \frac{\log(\log(y^2/s))}{(k-m+1)(k-m+2)} + \frac{\log(y^2/k)}{k-m+2}, \tag{41}$$

where $C = \frac{\log\left(\frac{D}{T_m L!} \frac{\Gamma(m-2)}{m^{m-2}}\right)}{(k-m+1)(k-m+2)} + \frac{\log(L-k)!}{k-m+1} - \frac{\log(L-k-1)!}{k-m+2}$, which is independent of y. Therefore, there exists r_0 such that if $y > \frac{1}{r_0}$, then $B_k \geq B_{k+1}$ for any $m \leq k < L$. The proof for $\{B_k\}_{m \leq k \leq L}$ in 3D can be derived similarly such that

$$\log B_k - \log B_{k+1} = \bar{C} + \frac{3m-6}{(k-m+1)(k-m+2)} \log y, \tag{42}$$

where $\bar{C} = \frac{\log\left(\frac{D}{T_m L! m^{1/3}} \left(\left(\frac{4}{3}\right)^{m-1} \sqrt{\frac{3\Gamma((3m-5)/2)}{\pi^{(m-1)}}} \frac{1}{2m^{(3m-4)/3}}\right)\right)}{(k-m+1)(k-m+2)} + \frac{\log\left((L-k)! k^{1/3} 2^{k-m}\right)}{k-m+1} - \frac{\log\left((L-k-1)!(k+1)^{1/3} 2^{k-m+1}\right)}{k-m+2}$. Thus, there exists r_0 such that, if $y > \frac{1}{r_0}$, the inequality $B_k \geq B_{k+1}$ holds for all $m \leq k < L$. □

Remark 9. Proposition 1 implies that

$$B_k \leq V < B_{k-1} \quad \text{if and only if} \quad \pi(\mathbf{x}_0) \leq \pi(\mathbf{x}_k) \tag{43}$$

for any $k \leq j \leq L$. Thus, if $V < B_m$, then $\pi(\mathbf{x}_0) > \pi(\mathbf{x}_k)$ for any $m \leq k \leq L$, which means that there is only one mode at state $\mathbf{x}_0$.

Now, we turn to the ranges of viscosity with which a local maximum of π is at $\mathbf{x}_k$.

Proposition 2. Suppose that $m \geq 5$, $P_{tot} = L$, and $L = 2m-1$ in (3). Then, there exists $\{G_k\}_{m \leq k < L}$ such that

$$G_k \leq V \quad \text{if and only if} \quad \pi(\mathbf{x}_k) \leq \pi(\mathbf{x}_{k+1}). \tag{44}$$

Furthermore, there exists r_0 such that $\{G_k\}_{m \leq k < L}$ is an increasing sequence if $r < r_0$, for each case 2D and 3D.

Proof. For any $m \geq 5$, by (8) and (37), we have that for any $m \leq k \leq L$,

$$\frac{\pi(\mathbf{x}_k)}{\pi(\mathbf{x}_0)} = \frac{L!}{(L-k)!} Q_k \geq 1 \tag{39}$$

for both 2D and 3D. Furthermore, there exists r_0 such that $\{B_k\}_{m \leq k \leq L}$ is a decreasing sequence if $r < r_0$ in both 2D and 3D.

Proof. For any $m \geq 5$, by (8) and (37), we have that for any $m \leq k \leq L$,

$$\frac{\pi(\mathbf{x}_{k+1})}{\pi(\mathbf{x}_k)} = \frac{(L-k)!}{(L-k-1)!} \frac{Q_{k+1}}{Q_k} \geq 1 \tag{45}$$

is equivalent to $G_k \leq V$, where

$$G_k = \begin{cases} \frac{y^2 \ln(y^2/k)}{(L-k)} & \text{if } d=2, \\ \frac{2y^3}{(L-k)} \left(\frac{k+1}{k}\right)^{1/3} & \text{if } d=3. \end{cases} \tag{46}$$

By simple calculation, in 2D, we find that if $y \geq \sqrt{\frac{1}{2(m-1)(1+m^{-1})^{m-1}}}$, then for any $m \leq k < L$,

$$\frac{G_{k+1}}{G_k} = \frac{(L-k)}{(L-k-1)} \frac{\ln(y^2/(k+1))}{\ln(y^2/k)} \geq 1. \tag{47}$$

Hence, for $r_0 = 1/\sqrt{(L-1)(1+m^{-1})^{L-m}}$, the results hold in 2D. Similarly, in 3D, we find that for any $5 \leq m \leq k < L$,

$$\frac{G_{k+1}}{G_k} = \frac{(L-k)}{(L-k-1)} \left[\frac{k(k+2)}{(k+1)^2}\right]^{\frac{1}{3}} \geq \frac{m-1}{m-2} \left[\frac{m(m+2)}{(m+1)^2}\right]^{\frac{1}{3}} = \left(1 + \frac{3m^4 - 4m^3 - 5m^2 + 2m + 8}{(m-2)^3(m+1)^2}\right)^{\frac{1}{3}} > 1. \tag{48}$$

This implies that $\{G_k\}_{m \leq k < L}$ is also an increasing sequence in 3D for any choice of sufficiently small r. □

Remark 10. Proposition 2 implies that $G_k \leq V < G_{k-1}$ if and only if

$$\pi(\mathbf{x}_k) \leq \pi(\mathbf{x}_k) \tag{49}$$

for any $m \le j \le L$. Under this range of the viscosity, the stationary distribution has a local maximum at state $\mathbf{x}$. Moreover, by (32), we can see that for sufficiently small ϵ, G_k in 2D is smaller than G_k in 3D.

B. Theoretical validation for Sec. IV C

We demonstrate the effect of the threshold m for droplet formation in 2D and 3D by using the value of the stationary distributions at state $\mathbf{x}_0 = (P_{tot}, 0, 0, \ldots, 0)$ that do not include droplets. In the context of comparison, we will also use π^{2D} and π^{3D} to denote the stationary distribution in 2D and 3D, respectively. Through the probabilities $\pi^{2D}(\mathbf{x}_0)$ and $\pi^{3D}(\mathbf{x}_0)$, we prove that there exists a range of m for which $\pi^{3D}(\mathbf{x}_0)$ is much greater than $\pi^{2D}(\mathbf{x}_0)$. We first derive an inequality for the ratio of the probability of forming no droplets between 2D and 3D.

Proposition 3. Suppose that $m \ge 5$. For fixed $L \ge m$ and $P_{tot} \ge m$, we have that for any $r > 1$,

$$\frac{\pi^{3D}(\mathbf{x}_0)}{\pi^{2D}(\mathbf{x}_0)} \ge \frac{1 + y^{m-1}\sum_{\mathbf{x}\in S_{\mathbf{x}_0}/\{\mathbf{x}_0\}} \frac{\pi^{3D}(\mathbf{x})}{\pi^{3D}(\mathbf{x}_0)}}{1 + \sum_{\mathbf{x}\in S_{\mathbf{x}_0}/\{\mathbf{x}_0\}} \frac{\pi^{3D}(\mathbf{x})}{\pi^{3D}(\mathbf{x}_0)}}, \tag{50}$$

where $y = 1/r$.

Proof. Let $m \ge 5$ be fixed. By (8) and (37), we can derive that for any state $\mathbf{x} = (x_1, x_2, \ldots, x_L) \in S_{\mathbf{x}_0}/\{\mathbf{x}_0\}$,

$$\left(\frac{\pi^{2D}(\mathbf{x})}{\pi^{2D}(\mathbf{x}_0)}\right) \Big/ \left(\frac{\pi^{3D}(\mathbf{x})}{\pi^{3D}(\mathbf{x}_0)}\right) = \prod_{k=m}^{L} \left(\frac{Q_k^{2D}}{Q_k^{3D}}\right)^{x_k}. \tag{51}$$

For any $m \le k \le L$, the ratio Q_k of 2D to 3D is

$$\begin{aligned} Q_k^{2D}/Q_k^{3D} &= \Theta_m k^{1/3} \frac{y^{k-1}}{\left[\prod_{s=m}^{k-1} \ln(y/\sqrt{s})\right]} \\ &= \Theta_m k^{1/3} \frac{y^{k-m}}{\left[\prod_{s=m}^{k-1} \ln(y/\sqrt{s})\right]} y^{m-1} \\ &\ge \Theta_m k^{1/3} \sqrt{\frac{(k-1)!}{(m-1)!}} y^{m-1} \ge \Theta_m m^{1/3} y^{m-1}, \end{aligned} \tag{52}$$

where $y = 1/r$ and

$$\Theta_m = \frac{\Gamma((3m-5)/2)}{\Gamma(m-2)} \left(\frac{4}{3}\right)^{m-2} \frac{2}{m\sqrt{\pi^{(m-1)}}}. \tag{53}$$

For simplicity, we let $\ell = m - 2$ and define $h(\ell) = \Theta_m m^{1/3}$. Based on Ref. 77, which presents the lower and upper bounds of the gamma function, we have

$$h(\ell) > \frac{\left(\frac{3\ell+1}{2}\right)^{\frac{3\ell}{2}}}{\ell^{\ell-1/2}} \frac{1}{e^{\frac{\ell}{2}+\frac{1}{12\ell}+\frac{1}{2}}} \left(\frac{2}{3}\right)^{\ell} \frac{1}{(\ell+2)^{2/3}} := \bar{h}(\ell). \tag{54}$$

Note that $\bar{h}(\ell)$ is the non-negative function for all $\ell \ge 1$ with $\bar{h}(3) \ge 1$. By analyzing the derivative of $\log \bar{h}(\ell)$, we will show that $\bar{h}(\ell)$ is an increasing function as $\ell \ge 3$. In particular, we have

$$\begin{aligned} \frac{d}{d\ell} \log \bar{h}(\ell) &= \left[\log\left(1 + \frac{1}{3\ell}\right) + \frac{1}{12\ell^2} + \frac{1}{2\ell}\right] \\ &\quad + \frac{1}{2} \log\left(\frac{3\ell+1}{2}\right) - \frac{21\ell+22}{6(\ell+2)(3\ell+1)}. \end{aligned} \tag{55}$$

This expression can be bounded by the sum of two increasing functions for $\ell \ge 3$ as follows:

$$\frac{d}{d\ell} \log \bar{h}(\ell) \ge \frac{1}{2} \log\left(\frac{3\ell+1}{2}\right) + \frac{(-21\ell-22)}{6(\ell+2)(3\ell+1)}. \tag{56}$$

Through some elementary calculations, we can show that $\frac{d}{d\ell} \log \bar{h}(\ell) > 0$. This implies that $\log \bar{h}(\ell)$ is an increasing function of ℓ for $\ell \ge 3$. Consequently, we have that $\bar{h}(\ell)$ is an increasing function, which finally implies $h(\ell) \ge 1$ for any $\ell \ge 3$ by (54).

Since for each $\mathbf{x} = (x_1, x_2, \ldots, x_L) \in S_{\mathbf{x}_0}/\{\mathbf{x}_0\}$, it must hold that $x_k \ge 1$ for at least one $k \ge m$. Therefore, by (51) and (52),

$$\frac{\pi^{2D}(\mathbf{x})}{\pi^{2D}(\mathbf{x}_0)} \ge y^{m-1} \frac{\pi^{3D}(\mathbf{x})}{\pi^{3D}(\mathbf{x}_0)} \tag{57}$$

for any $\mathbf{x} \in S_{\mathbf{x}_0}/\{\mathbf{x}_0\}$. We now establish the following equality:

$$\begin{aligned} \sum_{\mathbf{x}\in S_{\mathbf{x}_0}} \pi(\mathbf{x}) &= \pi(\mathbf{x}_0) \sum_{\mathbf{x}\in S_{\mathbf{x}_0}} \frac{\pi(\mathbf{x})}{\pi(\mathbf{x}_0)} \\ &= \pi(\mathbf{x}_0) \left(1 + \sum_{\mathbf{x}\in S_{\mathbf{x}_0}/\{\mathbf{x}_0\}} \frac{\pi(\mathbf{x})}{\pi(\mathbf{x}_0)}\right) = 1. \end{aligned} \tag{58}$$

So, we conclude that by (57),

$$\frac{\pi^{3D}(\mathbf{x}_0)}{\pi^{2D}(\mathbf{x}_0)} = \frac{1 + \sum_{\mathbf{x}\in S_{\mathbf{x}_0}/\{\mathbf{x}_0\}} \frac{\pi^{2D}(\mathbf{x})}{\pi^{2D}(\mathbf{x}_0)}}{1 + \sum_{\mathbf{x}\in S_{\mathbf{x}_0}/\{\mathbf{x}_0\}} \frac{\pi^{3D}(\mathbf{x})}{\pi^{3D}(\mathbf{x}_0)}} \tag{59}$$

$$\ge \frac{1 + y^{m-1}\sum_{\mathbf{x}\in S_{\mathbf{x}_0}/\{\mathbf{x}_0\}} \frac{\pi^{3D}(\mathbf{x})}{\pi^{3D}(\mathbf{x}_0)}}{1 + \sum_{\mathbf{x}\in S_{\mathbf{x}_0}/\{\mathbf{x}_0\}} \frac{\pi^{3D}(\mathbf{x})}{\pi^{3D}(\mathbf{x}_0)}}. \tag{60}$$

□

Remark 11. Now, we show the existence of a range of m where the probability of forming no droplets is significantly different between 2D and 3D in the following remark. To highlight the dependence on m, in this section, we denote by π_m^{2D} and π_m^{3D} the stationary distribution of 2D-LLPS and 3D-LLPS, respectively.

Let $5 \le m_0 \le L$ such that

$$\sum_{\mathbf{x}\in S_{\mathbf{x}_0}^{m_0}/\{\mathbf{x}_0\}} \frac{\pi_{m_0}^{3D}(\mathbf{x})}{\pi_{m_0}^{3D}(\mathbf{x}_0)} \ge \alpha \tag{61}$$

for some $\alpha > 0$, where $S_{\mathbf{x}_0}^{m_0}$ is the state space for given m_0. Since $\frac{\pi_m(\mathbf{x})}{\pi_m(\mathbf{x}_0)}$ is obviously decreasing with respect to m for any $\mathbf{x} \in S_{\mathbf{x}_0}^{m}/\{\mathbf{x}_0\}$

and for both 2D and 3D, by Proposition (3), we have that for any $m \in \{5, \ldots, m_0\}$,

$$\frac{\pi_m^{3D}(\mathbf{x}_0)}{\pi_m^{2D}(\mathbf{x}_0)} \geq \frac{1 + y^{m-1} \sum_{\mathbf{x} \in S_{\mathbf{x}_0}^m / \{\mathbf{x}_0\}} \frac{\pi_m^{3D}(\mathbf{x})}{\pi_m^{3D}(\mathbf{x}_0)}}{1 + \sum_{\mathbf{x} \in S_{\mathbf{x}_0}^m / \{\mathbf{x}_0\}} \frac{\pi_m^{3D}(\mathbf{x})}{\pi_m^{3D}(\mathbf{x}_0)}} \geq \frac{1 + y^{m-1}\alpha}{1 + \alpha}. \tag{62}$$

Here, for the second inequality, we used that the function $f(z) = \frac{1+\beta z}{1+z}$ is increasing for $z > 0$ when $\beta > 1$. For instance, suppose that there exists m_0 such that (61) holds with $\alpha = 1/2$. This roughly means that m_0 is not too big so that $\pi_{m_0}^{3D}(\mathbf{x}_0)$ is relative higher than $\pi_{m_0}^{3D}(\mathbf{x})$ for $\mathbf{x} \in S_{\mathbf{x}_0}^{m_0} / \{\mathbf{x}_0\}$. In this case, Proposition 3 implies that for each $m \in \{5, \ldots, m_0\}$, we have

$$\frac{\pi_m^{3D}(\mathbf{x}_0)}{\pi_m^{2D}(\mathbf{x}_0)} \geq \frac{1 + 0.5 y^{m-1}}{1.5}, \tag{63}$$

where $\frac{1+0.5y^{m-1}}{1.5}$ is a large number if $y = 1/r$ is sufficiently large.

C. Theoretical validation for Sec. IV D

We explore a sufficient condition for the fold-change constant $H \geq 1$, which enhances the probability of forming droplets in 3D, when the radius is reduced by anchoring a protein in 2D. This condition is defined by the ratio $r^{3D}/r^{2D} = H$, where r^{2D} and r^{3D} represent the hydrodynamic radii of individual proteins in 2D and 3D, respectively.

Proposition 4. Suppose that $m \geq 5$ and $m \leq P_{tot}$. Then, for each r^{2D}, there exists H^* such that

$$1 - \pi^{3D}(\mathbf{x}_0) \geq 1 - \pi^{2D}(\mathbf{x}_0) \tag{64}$$

if $H \geq H^*$, where $\mathbf{x}_0 = (P_{tot}, 0, \ldots, 0)$.

Proof. By (37), for any $m \leq k \leq L$, we have

$$Q_k^{3D} / Q_k^{2D} = \frac{H^{3k-3}}{\Theta_m \alpha_k} \geq 1, \tag{65}$$

where $\alpha_k = k^{1/3}\left[\frac{y^{k-1}}{\prod_{s=m}^{k-1} \ln(y\sqrt{s})}\right]$ with $y = 1/r^{2D}$ and Θ_m is defined as (53). For each $m \leq k \leq L$, we define the sequence $H_k = (\Theta_m \alpha_k)^{1/(3k-3)}$, which satisfies the following equivalence condition:

$$H \geq H_k \quad \text{if and only if} \quad Q_k^{3D} / Q_k^{2D} \geq 1. \tag{66}$$

Let $H^* := \max_{m \leq k \leq L} H_k$. By the definition of (8),

$$1 - \pi^{3D}(\mathbf{x}_0) \geq 1 - \pi^{2D}(\mathbf{x}_0)$$

if $H \geq H^*$, where $\mathbf{x}_0 = (P_{tot}, 0, \ldots, 0)$. □

Remark 12. We found that there exists r_0 such that $\{H_k\}_{m \leq k \leq L}$ is a decreasing sequence if $r^{2D} < r_0$ [Fig. 7(c)]. For any $m \leq k < L$, we show that $\log(H_k / H_{k+1})$ is non-negative as follows:

$$\log H_k - \log H_{k+1} = \Theta_1 + \frac{(k-1)\log(\log(y\sqrt{k})) - \sum_{s=m}^{k-1} \log(\log(y\sqrt{s}))}{3k(k-1)} \tag{67}$$

$$\geq \Theta_1 + \frac{\left[\log\left(\frac{\log(y\sqrt{k})}{\log(y\sqrt{m})}\right) + (m-1)\log\log(y\sqrt{k})\right]}{3k(k-1)}, \tag{68}$$

where $\Theta_1 = \frac{\log \Theta_m^3 + \log[k(k/k+1)^{k-1}]}{9k(k-1)}$ and $y = 1/r^{2D}$. Since, for any $\alpha, \beta > 0$, $\lim_{y \to \infty} \frac{\log(y/\alpha)}{\log(y/\beta)} = 1$, there exists r_0 such that $H_k \geq H_{k+1}$ for any $m \leq k \leq L$ if $y > \frac{1}{r_0}$, i.e., $H^* = \max_{m \leq k \leq L} H_k = H_m$.

Consequently, for each $\ell \neq k$,

$$\frac{Q_\ell^{3D}}{Q_\ell^{2D}} = \frac{\pi^{3D}(\mathbf{x}_\ell)/\pi^{3D}(\mathbf{x}_0)}{\pi^{2D}(\mathbf{x}_\ell)/\pi^{2D}(\mathbf{x}_0)} \geq 1 \text{ if and only if } H \geq H_k. \tag{69}$$

In the simple state space (29), if $H = H_L$, then $\pi^{3D}(\mathbf{x}_L)/\pi^{3D}(\mathbf{x}_0)$, the probability of forming the largest droplet in 3D relatively to the probability of no droplets, is bigger than or equal to $\pi^{2D}(\mathbf{x}_L)/\pi^{2D}(\mathbf{x}_0)$. However, for $\pi^{3D}(\mathbf{x}_L)/\pi^{3D}(\mathbf{x}_0) \geq \pi^{2D}(\mathbf{x}_L)/\pi^{2D}(\mathbf{x}_0)$, a bigger reduction in the hydrodynamic radius in 2D is needed as it holds only if $H \geq H_m > H_L$.

VI. CONCLUSION

We used a reaction network and the associated Markov chains to study how spatial dimension affects LLPS. We set the rate constants using the concepts of mean first passage times and generalized Smoluchowski reaction kinetics. These rate constants capture spatial dimensional effects, and they further reflect the physical influence of temperature on protein interaction range and viscosity in hydrodynamics. Using chemical reaction network theory, we obtained a closed form of the stationary distribution and revealed qualitative differences between 2D-LLPS and 3D-LLPS using this closed form.

Our model successfully reproduces the phase diagram of LLPS as predicted by free energy. Building on this validation, we performed an analytical and numerical investigation into viscosity in both 2D and 3D. This investigation shows that 2D-LLPS can form droplets at lower viscosities compared to 3D-LLPS. Furthermore, there exists a range of the threshold number of proteins required for droplet formation in which 2D-LLPS has a much higher probability of forming droplets than 3D-LLPS. This may provide a reason why cells utilize 2D spaces such as ER membranes for LLPS. Finally, considering the effect of the hydrodynamic radius of proteins, our paper identifies the ratio of the radii between 2D and 3D for which 3D-LLPS can have a similar number of droplets compared to 2D systems, and this result is supported by an analytical proof.

The Markov model we proposed is based on the first passage times of diffusing particles. While we primarily analyzed the stationary distribution of the model, there are many avenues for future work analyzing other aspects of the model. For instance, one can use chemical reaction network theory and present the Markov process using the random time representation[28] to study the diffusion limit

and the fluid limit of the model under the volume scaling and time scaling in future studies. Furthermore, the random-time representation and the Gillespie algorithm can also be employed to explore the transient dynamic of LLPS such as quasi-stationary behaviors and the pre-equilibrium behaviors. As such, our Markovian chemical reaction network theory of LLPS offers a new framework for studying a variety of microscopic (or mesoscopic) perspectives on LLPS.

As in all mathematical models of biophysical systems, we made a number of simplifying assumptions. For instance, we assumed Markovian dynamics with simple diffusion to highlight the effects of spatial dimensions. However, it is well established that protein motion often follows anomalous diffusion due to molecular crowding, resulting in subdiffusion and a loss of the Markov property.[79,80] Incorporating subdiffusion and non-Markovian effects into our model would be an interesting direction for future research. In addition, further insights could be provided by considering the spatial distributions of proteins using approaches similar to the Kawasaki–Glauber model from statistical mechanics,[81–83] which account for the positioning of individual particles and clusters. Our model has the potential to be extended in these ways, and exploring such factors will help move us toward a more comprehensive understanding of LLPS.

ACKNOWLEDGMENTS

The first and third authors were supported by the National Research Foundation of Korea (NRF) grant funded by the Korea government (MSIT) (Grant Nos. 2022R1C1C1008491 and RS-2023-00219980). The first author was also supported by the NRF grant funded by MSIT (Grant No. NRF-2017R1A5A1015366). The third author was also supported by the NRF grant funded by MSIT (Grant No. 2021R1A6A1A10042944), POSCO HOLDINGS research fund (Grant No. 2022Q019), and Samsung Electronics Co., Ltd. (Grant No. IO230407-05812-01). The second author was supported by the National Science Foundation (Grant Nos. DMS-2325258 and CAREER DMS-1944574). We thank Professor Joo-Yeon Yoo (POSTECH) and Dr. Nari Kim (POSTECH) for inspiring discussions.

AUTHOR DECLARATIONS

Conflict of Interest

The authors have no conflicts to disclose.

Author Contributions

J.K. analyzed the model, performed the numerical simulations, made figures, and wrote the manuscript. S.D.L. provided key details of the model and edited the manuscript. J.K. initiated the project, developed the model, and wrote the manuscript.

Jinyoung Kim: Conceptualization (equal); Formal analysis (equal); Methodology (equal); Visualization (lead); Writing – original draft (equal); Writing – review & editing (equal). **Sean D. Lawley**: Conceptualization (supporting); Validation (equal); Writing – original draft (supporting); Writing – review & editing (equal). **Jinsu Kim**: Conceptualization (lead); Funding acquisition (equal); Methodology (equal); Supervision (lead); Writing – original draft (equal); Writing – review & editing (equal).

DATA AVAILABILITY

Data sharing is not applicable to this article as no new data were created or analyzed in this study.

APPENDIX A: MODELING DETAILS

Here, we give more details pertaining to modeling LLPS with the stochastically modeled reaction network (3).

1. The minimum number of proteins for droplet formation

The minimal number of proteins, m, for droplet formation is experimentally and theoretically validated in Refs. 51, 84, and 85. In Ref. 51, the authors used the condition of zero flux to derive the critical number of proteins to form the nucleation barrier. We can also validate the existence of the minimal number with our Markov model and the volume fraction (27). As shown in Fig. 8 (right), the volume fraction with $m = 3$ (that is, assuming that a droplet can be formed with three proteins) immediately increases when P_{tot} increases, as opposed to the case of $m = 10$ displayed in Fig. 8 (left), where the plateau of the volume fraction characterizes the existence of the threshold protein concentration for phase separation. This indicates that if an arbitrarily small number (such as ≤ 3) of proteins can form droplets, then there is no threshold concentration of the protein to form droplets. Hence, the condition of $m \geq 3$ fails to capture the key feature of LLPS.

2. Ostwald ripening

If some proteins are dissociated from a droplet, the balance between the influx and the outflow of the droplet can collapse. This leads to the dilution of the dense state and is modeled by $D_m \to mP$. This reaction also models Ostwald ripening, which is another mechanism to grow the size of droplets rather than coalescence and fusion. According to Ostwald ripening, small droplets disappear through the reaction $D \to mP$, which leads to dilution due to higher flux (or higher Laplace pressure) of small droplets and the proteins. In other words, the molecules on the surface of a smaller droplet are energetically less stable compared to those in larger droplets. Hence, the inside proteins leave the droplet.[86] These proteins diffuse and merge into large droplets as $D_k \to D_{k+1}$ for some k.

3. Protein assembly and LLPS

Protein assembly and phase separation are distinct concepts.[3] Proteins can not only form droplets but also assemble with other proteins.[2,38] Multiple monomers can assemble to create a multimer. A thermodynamical point of view revealed that the size distribution of protein assemblies can change the configuration of LLPS.[38]

Therefore, it is meaningful to model such assembly processes with reactions $P_i + P_j \to D \to P_{i+j}$, where P_i represents i-mers. However, to build a more coarser-grained model, we assume that the assembly process is on a much slower timescale compared to the

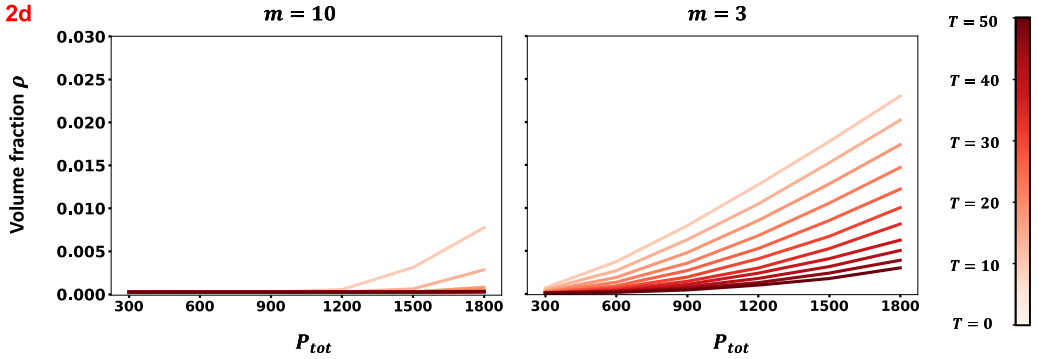

FIG. 8. Validation of the necessity of $m > 3$ using the volume fraction. Volume fractions (27) as a function of P_{tot} for $m = 10$ and $m = 3$. Only the case of $m = 10$ displays a plateau on the range of small values P_{tot} that characterizes the threshold protein concentration for droplet formation.

timescale of phase separation. This setting is also used in Ref. 38. Another possible scenario is that the assembly equilibrium is already made so that the process of the protein assembly is less dynamical than phase separation. Hence, we can average out the effect of the size distribution of the assemblies. In those scenarios, we assume that P represents the number of total proteins including both monomers and multimers.

4. Mass-action kinetics under well-mixed compartments

Phase separation obviously makes the space demixed. However, each compartment can be well-mixed. That is, the space on a diluted phase is well-mixed and the inner space of droplets is also well-mixed. This condition is essential for the reactions to take place in either dilute spaces or dense spaces. Under this condition of well-mixed compartments, it is reasonable to use mass-action kinetics for the reactions in (3).

5. Mobilities of droplets and the proteins in the dense phase

As droplet mass increases, the diffusion coefficient of proteins inside the droplets decreases, which causes small mobility of droplets. In addition, an existing study provided a more precise comparison between proteins inside and outside droplets.[8] The authors experimentally found that the molecular rearrangement rate of membrane-bound proteins is slower within droplets compared to the same proteins outside the droplets.[14,52] This motivated us to assume that droplet fusion and fission events occur at a much slower rate than droplet formation, coarsening, and dissociation events. Thus, we ignore fusion and fission in our model. Note that we incorporate the disparity of protein mobilities into the reaction rate constants with the constant V in the rates k_b.

6. Multicomponent LLPS

LLPS often takes place with multiple proteins as scaffold proteins drive phase separation and clients are engaged into it.[87] We consider a single type of scaffold proteins in this work for the sake of simplicity.

7. Temperature effects on the volume fraction and the phase diagram

The temperature effect in the phase diagram can be explained as follows. Due to a low viscosity with high temperature, a higher number of proteins are needed to initiate forming droplets and maintaining them. However, a longer hydrodynamic radius with high temperature makes the volume of the droplets bigger so that the ratio of the droplet volume can easily be large with high temperature.

APPENDIX B: PARAMETERS IN ALL FIGURES

We provide the values of the parameters we used in Table I. The temperature T is measured in Celsius. The following functions are used to generate all figures:

$$V = V_0 \cdot e^{\frac{8500}{T+273}},$$

$$r = r_0 \cdot (T + 273).$$

In general, we use a diffusion coefficient for both 2D and 3D, $D^{2D} = D^{3D} = 1$, and set the system size to $R = 1$ for all figures. However, for Fig. 3(c), we used $D^{2D} = 10\ \mu m^2 s^{-1}$ as found in Ref. 14, a system size of $R = 10^3\ \mu m$ and $r = 5\ \mu m$ at $T = 36$ based on an existing study. For Fig. 8, time trajectories are sampled using the same algorithm and initial state described for 2D in Fig. 4 with the sampling process terminated after 10^4 reactions for both $m = 3$ and $m = 10$.

APPENDIX C: DERIVATION OF STATIONARY DISTRIBUTIONS

In the literature of chemical reaction network theory, researchers use structural properties of chemical reaction networks to derive the dynamical features of the associated dynamical systems for the chemical reaction networks. The following theorem (Theorem 4.2 in Ref. 56) shows that a certain structural property can imply a closed form of the stationary distribution of the associated Markov chain.

Theorem 1. *Let X be the associated continuous-time Markov chain for a chemical reaction network whose connected components are strongly connected. Let n and ℓ denote the numbers of the*

TABLE I. Parameter values for all figures.

Parameters	Definition	Figures							
		1	3	4	5(d)	6	7	8	9
m	Threshold			10		[5, 35]	10	3, 10	10
L	The number of proteins in the largest droplets			19		36	19	19	19
V_0	Viscosity scaling constant	e^{-25}	e^{-19}	e^{-25}		e^{-6}	e^{-12}		e^{-25}
T	Temperature	36		[0, 50]	36	10, 36, 60	36		[0, 50]
$\frac{r_0}{R}$	Hydrodynamic radius/system size	$\frac{5\cdot10^{-3}}{309}$	. . .				$\frac{5\cdot10^{-3}}{309}$		
P_{tot}	Total proteins	. .	$5\cdot10^4$	(2D) $[5\cdot10^2, 8\cdot10^3]$ & $[1.5\cdot10^4, 3\cdot10^4]$ (3D) $[10^5, 2.3\cdot10^5]$ & $[45\cdot10^5, 85\cdot10^5]$	200	100	19	(2D) $[3\cdot10^2, 18\cdot10^2]$	(2D) $8\cdot10^3$, $1.5\cdot10^4$, and $3\cdot10^4$ (3D) $23\cdot10^5$, $45\cdot10^5$, and $65\cdot10^5$

nodes and the connected components of the chemical reaction network, respectively. Furthermore, let s be the dimension of the vector space span$\{y_k - y_k : y_k \to y_k\}$. For $X(0) = \mathbf{x}_0$, if $n - \ell - s = 0$, then X admits a unique stationary distribution π such that for each state $\mathbf{x}$,

$$\lim_{t\to\infty} P(X(t) = \mathbf{x}) = \pi(\mathbf{x}) = M \prod_{i=1}^{d} \frac{c_i^{\mathbf{x}}}{\mathbf{x}!}, \qquad \text{(C1)}$$

where c is any positive steady state of a system of ordinary differential equations given by

$$\frac{d}{dt}x(t) = \sum_{y\to y'} \prod_{i=1}^{d} (x_i(t))^{y_i}(y' - y),$$

where M is the normalizing constant $M = \left(\sum_{\mathbf{x}\in S_{\mathbf{x}_0}} \prod_{i=1}^{d} \frac{c_i^{\mathbf{x}}}{\mathbf{x}!}\right)^{-1}$, and $S_{\mathbf{x}_0}$ is the closed communication class containing $\mathbf{x}_0$.

We now clarify some terminology in Theorem 1. We first define connected components as the typical concept in graph theory

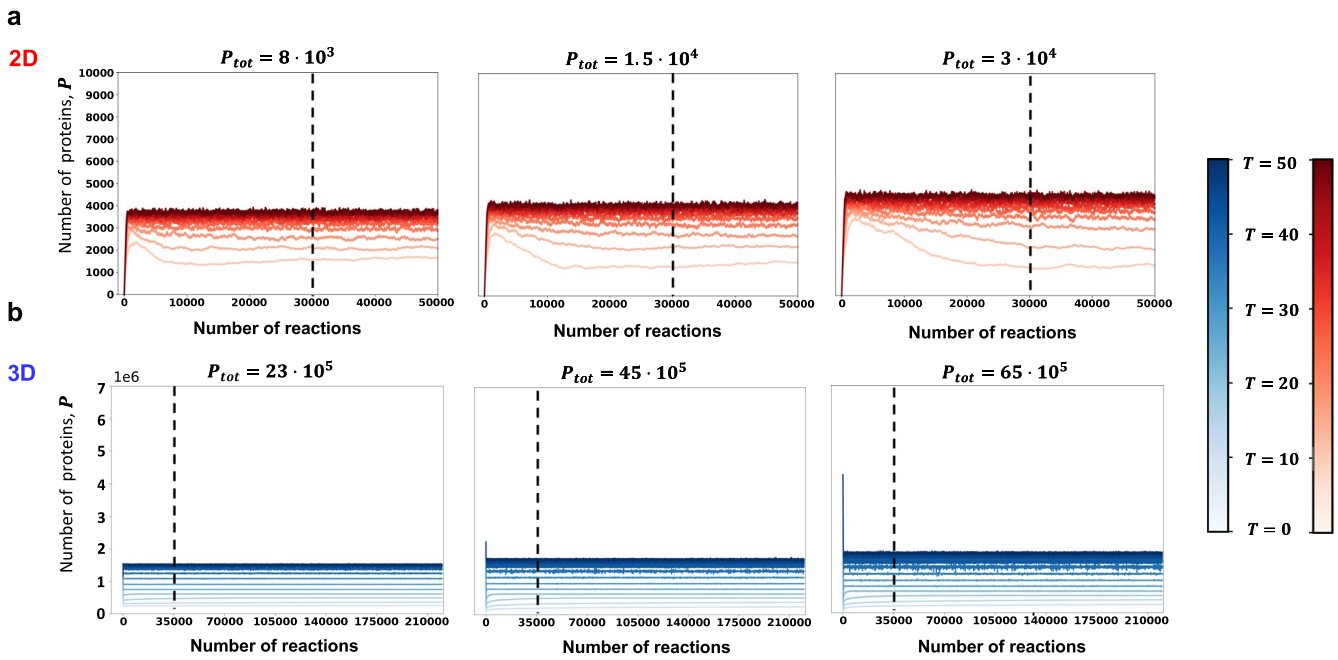

FIG. 9. Convergence of trajectories. The time trajectories with the different total numbers of proteins P_{tot} and the different choices of the temperatures for 2D (top) and 3D (bottom).

regarding the chemical reaction network as a graph. A connected component is strongly connected if, whenever there exists a path from node v to node u in the component, then there is also a path from node u to v in the connected component. For example, in the following reaction network,

$$A \longrightarrow B \qquad 2C \longrightarrow D$$
$$\nwarrow \swarrow \qquad \searrow \swarrow$$
$$C \qquad 2B$$

the first connected component is strongly connected, but the second one is not.

Remark 13. There are $n = 2L - 2m + 2$ nodes in (3) and $\ell = L - m + 1$ connected components, of which each is strongly connected. In addition, the reaction vectors are

$$\pm(-m, 1, 0, \ldots), \pm(-1, -1, 1, \ldots, 0), \ldots, \pm(-1, 0, \ldots, -1, 1).$$

Hence, the dimension of the vector space spanned by these reaction vectors is $s = L - m + 1$. Hence, $n - \ell - s = 0$. This implies that the closed form (8) of the stationary distribution of the Markov model is associated with (3).

APPENDIX D: APPROXIMATE π WITH SAMPLE TRAJECTORIES

The volume fractions and phase diagrams in Fig. 4 are estimated using the time trajectories sampled with Gillespie's algorithm (2D) and the tau-leaping method (3D).[76] In the simulation, the initial state is defined as

$$X(0) = \begin{cases} (0, P_{tot}/m, 0, \ldots, 0) & \text{if } d = 2, \\ (P_{tot}/2, P_{tot}/2m, 0, \ldots, 0) & \text{if } d = 3, \end{cases}$$

where the sampling process was terminated after $3 \cdot 10^4$ reactions in 2D simulations. For the 3D case, to reduce computational costs, we used the tau-leaping method and terminated the sampling at $3.5 \cdot 10^4$ reactions. Figure 9 shows that the samples closely approximate the volume fraction (27), as the number of proteins in the dilute phase (P_1) stabilizes when the specified number of reactions is fired.

REFERENCES

[1] S. Alberti, A. Gladfelter, and T. Mittag, "Considerations and challenges in studying liquid-liquid phase separation and biomolecular condensates," Cell **176**(3), 419–434 (2019).

[2] S. F. Banani, H. O. Lee, A. A. Hyman, and M. K. Rosen, "Biomolecular condensates: Organizers of cellular biochemistry," Nat. Rev. Mol. Cell Biol. **18**(5), 285–298 (2017).

[3] C. P. Brangwynne, C. R. Eckmann, D. S. Courson, A. Rybarska, C. Hoege, J. Gharakhani, F. Jülicher, and A. A. Hyman, "Germline P granules are liquid droplets that localize by controlled dissolution/condensation," Science **324**(5935), 1729–1732 (2009).

[4] A. A. Hyman, C. A. Weber, and F. Jülicher, "Liquid-liquid phase separation in biology," Annu. Rev. Cell Dev. Biol. **30**, 39–58 (2014).

[5] Y. Shin and C. P. Brangwynne, "Liquid phase condensation in cell physiology and disease," Science **357**(6357), eaaf4382 (2017).

[6] H.-L. Liu, H. Nan, W. W. Zhao, X.-B. Wan, and X.-J. Fan, "Phase separation in DNA double-strand break response," Nucleus **15**(1), 2296243 (2024).

[7] B. R. Levone, S. C. Lenzken, M. Antonaci, A. Maiser, A. Rapp, F. Conte, S. Reber, J. Mechtersheimer, A. E. Ronchi, O. Mühlemann *et al.*, "FUS-dependent liquid–liquid phase separation is important for DNA repair initiation," J. Cell Biol. **220**(5), e202008030 (2021).

[8] J. Miné-Hattab, S. Liu, and A. Taddei, "Repair foci as liquid phase separation: Evidence and limitations," Genes **13**(10), 1846 (2022).

[9] N. Kim, T.-H. Kim, C. Kim, J.-E. Lee, M.-G. Kang, S. Shin, M. Jung, J.-S. Kim, J. Y. Mun, H.-W. Rhee *et al.*, "Intrinsically disordered region-mediated condensation of IFN-inducible SCOTIN/SHISA-5 inhibits ER-to-Golgi vesicle transport," Dev. Cell **58**(19), 1950–1966.e8 (2023).

[10] S. Mehta and J. Zhang, "Liquid–liquid phase separation drives cellular function and dysfunction in cancer," Nat. Rev. Cancer **22**(4), 239–252 (2022).

[11] B. Wang, L. Zhang, T. Dai, Z. Qin, H. Lu, L. Zhang, and F. Zhou, "Liquid–liquid phase separation in human health and diseases," Signal Transduction Targeted Ther. **6**(1), 290 (2021).

[12] S. Wegmann, B. Eftekharzadeh, K. Tepper, K. M. Zoltowska, R. E. Bennett, S. Dujardin, P. R. Laskowski, D. MacKenzie, T. Kamath, C. Commins *et al.*, "Tau protein liquid–liquid phase separation can initiate tau aggregation," EMBO J. **37**(7), e98049 (2018).

[13] W. T. Snead and A. S. Gladfelter, "The control centers of biomolecular phase separation: How membrane surfaces, PTMs, and active processes regulate condensation," Mol. Cell **76**(2), 295–305 (2019).

[14] W. T. Snead, A. P. Jalihal, T. M. Gerbich, I. Seim, Z. Hu, and A. S. Gladfelter, "Membrane surfaces regulate assembly of ribonucleoprotein condensates," Nat. Cell Biol. **24**(4), 461–470 (2022).

[15] N. Kedersha, P. Ivanov, and P. Anderson, "Stress granules and cell signaling: More than just a passing phase?," Trends Biochem. Sci. **38**(10), 494–506 (2013).

[16] Y. Lin, D. S. W. Protter, M. K. Rosen, and R. Parker, "Formation and maturation of phase-separated liquid droplets by RNA-binding proteins," Mol. Cell **60**(2), 208–219 (2015).

[17] T. Hirose, K. Ninomiya, S. Nakagawa, and T. Yamazaki, "A guide to membraneless organelles and their various roles in gene regulation," Nat. Rev. Mol. Cell Biol. **24**(4), 288–304 (2023).

[18] J. A. Ditlev, "Membrane-associated phase separation: Organization and function emerge from a two-dimensional milieu," J. Mol. Cell Biol. **13**(4), 319–324 (2021).

[19] L. B. Case, "Membranes regulate biomolecular condensates," Nat. Cell Biol. **24**(4), 404–405 (2022).

[20] F. A. Thomas, I. Visco, Z. Peska, F. Heinemann, and P. Schwille, "Diffusion coefficients and dissociation constants of enhanced green fluorescent protein binding to free standing membranes," Data Brief **5**, 537–541 (2015).

[21] S. K. Zareh, M. C. DeSantis, J. M. Kessler, J.-L. Li, and Y. M. Wang, "Single-image diffusion coefficient measurements of proteins in free solution," Biophys. J. **102**(7), 1685–1691 (2012).

[22] G. Adam and M. Delbrück, "Reduction of dimensionality in biological diffusion processes," in *Structural Chemistry and Molecular Biology* (W.H. Freeman, 1968), p. 198.

[23] J. Norris, *Markov Chains* (Cambridge University Press, 1997).

[24] R. Durrett, *Essentials of Stochastic Processes*, 3rd ed. (Springer, 2016).

[25] C. E. Lawrence, *Partial Differential Equations* (American Mathematical Society, 2022), Vol. 19.

[26] M. J. Saxton, "Modeling 2d and 3d diffusion," in *Methods in Membrane Lipids* (Humana Press, 2007), pp. 295–321.

[27] W. Nadler and D. L. Stein, "Biological transport processes and space dimension," Proc. Natl. Acad. Sci. U. S. A. **88**(15), 6750–6754 (1991).

[28] S. M. Abel, J. P. Roose, J. T. Groves, A. Weiss, and A. K. Chakraborty, "The membrane environment can promote or suppress bistability in cell signaling networks," J. Phys. Chem. B **116**(11), 3630–3640 (2012).

[29] D. L. Shea, G. M. Omann, and J. J. Linderman, "Calculation of diffusion-limited kinetics for the reactions in collision coupling and receptor cross-linking," Biophys. J. **73**(6), 2949 (1997).

[30] B. N. Kholodenko, J. B. Hoek, and H. V. Westerhoff, "Why cytoplasmic signalling proteins should be recruited to cell membranes," Trends Cell Biol. **10**(5), 173–178 (2000).

[31] J. M. Haugh, "A unified model for signal transduction reactions in cellular membranes," Biophys. J. **82**(2), 591–604 (2002).
[32] M. I. Monine and J. M. Haugh, "Signal transduction at point-blank range: Analysis of a spatial coupling mechanism for pathway crosstalk," Biophys. J. **95**(5), 2172–2182 (2008).
[33] S. Alonso and M. Bär, "Phase separation and bistability in a three-dimensional model for protein domain formation at biomembranes," Phys. Biol. **7**(4), 046012 (2010).
[34] S. D. Lawley and J. P. Keener, "Including rebinding reactions in well-mixed models of distributive biochemical reactions," Biophys. J. **111**, 2317–2328 (2016).
[35] S. D. Lawley and J. P. Keener, "Rebinding in biochemical reactions on membranes," Phys. Biol. **14**(5), 056002 (2017).
[36] M. G. Dixon and J. P. Keener, "Dimensional dependence of binding kinetics," Bull. Math. Biol. **86**(8), 87 (2024).
[37] D. S. Grebenkov, R. Metzler, and G. Oshanin, "Search efficiency in the Adam–Delbrück reduction-of-dimensionality scenario versus direct diffusive search," New J. Phys. **24**(8), 083035 (2022).
[38] G. Bartolucci, I. S. Haugerud, T. C. T. Michaels, and C. A. Weber, "The interplay between biomolecular assembly and phase separation," eLife **13**, RP93003 (2024).
[39] C. P. Brangwynne, P. Tompa, and R. V. Pappu, "Polymer physics of intracellular phase transitions," Nat. Phys. **11**(11), 899–904 (2015).
[40] H. Falahati and A. Haji-Akbari, "Thermodynamically driven assemblies and liquid–liquid phase separations in biology," Soft Matter **15**(6), 1135–1154 (2019).
[41] J. W. Cahn and J. E. Hilliard, "Free energy of a nonuniform system. I. Interfacial free energy," J. Chem. Phys. **28**(2), 258–267 (1958).
[42] S. M. Allen and J. W. Cahn, "A microscopic theory for antiphase boundary motion and its application to antiphase domain coarsening," Acta Metall. **27**(6), 1085–1095 (1979).
[43] D. Jacqmin, "Calculation of two-phase Navier–Stokes flows using phase-field modeling," J. Comput. Phys. **155**(1), 96–127 (1999).
[44] X. Zhang, X. Man, C. C. Han, and D. Yan, "Nucleation induced by phase separation in the interface of polyolefin blend," Polymer **49**(9), 2368–2372 (2008).
[45] K. Gasior, M. G. Forest, A. S. Gladfelter, and J. M. Newby, "Modeling the mechanisms by which coexisting biomolecular RNA–protein condensates form," Bull. Math. Biol. **82**, 153 (2020).
[46] K. Gasior, J. Zhao, G. McLaughlin, M. G. Forest, A. S. Gladfelter, and J. Newby, "Partial demixing of RNA-protein complexes leads to intradroplet patterning in phase-separated biological condensates," Phys. Rev. E **99**(1), 012411 (2019).
[47] E. W. Hester, S. Carney, V. Shah, A. Arnheim, B. Patel, D. Di Carlo, and A. L. Bertozzi, "Fluid dynamics alters liquid–liquid phase separation in confined aqueous two-phase systems," Proc. Natl. Acad. Sci. U. S. A. **120**(49), e2306467120 (2023).
[48] H. Yu, S. Lu, K. Gasior, D. Singh, S. Vazquez-Sanchez, O. Tapia, D. Toprani, M. S. Beccari, J. R. Yates III, S. Da Cruz *et al.*, "HSP70 chaperones RNA-free TDP-43 into anisotropic intranuclear liquid spherical shells," Science **371**(6529), eabb4309 (2021).
[49] A. Girelli, H. Rahmann, N. Begam, A. Ragulskaya, M. Reiser, S. Chandran, F. Westermeier, M. Sprung, F. Zhang, C. Gutt, and F. Schreiber, "Microscopic dynamics of liquid-liquid phase separation and domain coarsening in a protein solution revealed by x-ray photon correlation spectroscopy," Phys. Rev. Lett. **126**(13), 138004 (2021).
[50] K. L. Saar, D. Qian, L. L. Good, A. S. Morgunov, R. Collepardo-Guevara, R. B. Best, and T. P. J. Knowles, "Theoretical and data-driven approaches for biomolecular condensates," Chem. Rev. **123**(14), 8988–9009 (2023).
[51] E. W. Martin, T. S. Harmon, J. B. Hopkins, S. Chakravarthy, J. J. Incicco, P. Schuck, A. Soranno, and T. Mittag, "A multi-step nucleation process determines the kinetics of prion-like domain phase separation," Nat. Commun. **12**(1), 4513 (2021).
[52] K. Kamagata, N. Iwaki, S. Kanbayashi, T. Banerjee, R. Chiba, V. Gaudon, B. Castaing, and S. Sakomoto, "Structure-dependent recruitment and diffusion of guest proteins in liquid droplets of FUS," Sci. Rep. **12**(1), 7101 (2022).
[53] J. M. Ball and J. Carr, "Asymptotic behaviour of solutions to the Becker-Doring equations for arbitrary initial data," Proc. R. Soc. Edinburgh, Sect. A **108**, 109–116 (1988).
[54] E. Hingant and R. Yvinec, "Deterministic and stochastic Becker-Döring equations: Past and recent mathematical developments," in *Stochastic Processes, Multiscale Modeling, and Numerical Methods for Computational Cellular Biology* (Springer, 2016), pp. 175–204.
[55] E. Hingant and R. Yvinec, "Quasi-stationary distribution and metastability for the stochastic Becker-Döring model," Electron. Commun. Probab. **26**, 1–14 (2021).
[56] D. F. Anderson, G. Craciun, and T. G. Kurtz, "Product-form stationary distributions for deficiency zero chemical reaction networks," Bull. Math. Biol. **72**(8), 1947–1970 (2010).
[57] N. A. Yewdall, A. A. M. André, T. Lu, and E. Spruijt, "Coacervates as models of membraneless organelles," Curr. Opin. Colloid Interface Sci. **52**, 101416 (2021).
[58] S. Qin and H.-X. Zhou, "Protein folding, binding, and droplet formation in cell-like conditions," Curr. Opin. Struct. Biol. **43**, 28–37 (2017).
[59] M. B. Flegg, "Smoluchowski reaction kinetics for reactions of any order," SIAM J. Appl. Math. **76**(4), 1403–1432 (2016).
[60] J. B. Madrid and S. D. Lawley, "Competition between slow and fast regimes for extreme first passage times of diffusion," J. Phys. A: Math. Theor. **53**(33), 335002 (2020).
[61] M. V. Smoluchowski, "Versuch einer mathematischen theorie der koagulationskinetik kolloider lösungen," Z. Phys. Chem. **92U**(1), 129–168 (1918).
[62] D. Shoup and A. Szabo, "Role of diffusion in ligand binding to macromolecules and cell-bound receptors," Biophys. J. **40**, 33–39 (1982).
[63] C. B. Paul, *Stochastic Processes in Cell Biology* (Springer, 2014), Vol. 41.
[64] A. A. Polyansky, L. D. Gallego, R. G. Efremov, A. Köhler, and B. Zagrovic, "Protein compactness and interaction valency define the architecture of a biomolecular condensate across scales," Elife **12**, e80038 (2023).
[65] Y. C. Kim, R. B. Best, and J. Mittal, "Macromolecular crowding effects on protein–protein binding affinity and specificity," J. Chem. Phys. **133**(20), 205101 (2010).
[66] F. Muzzopappa, J. Hummert, M. Anfossi, S. A. Tashev, D.-P. Herten, and F. Erdel, "Detecting and quantifying liquid–liquid phase separation in living cells by model-free calibrated half-bleaching," Nat. Commun. **13**(1), 7787 (2022).
[67] D. Lee, J. Kim, and G. Lee, "Simple methods to determine the dissociation constant, K_d," Mol. Cells **47**, 100112 (2024).
[68] S. Banjade and M.K. Rosen, "Phase transitions of multivalent proteins can promote clustering of membrane receptors," elife **3**, e04123 (2014).
[69] P. Li, S. Banjade, H.-C. Cheng, S. Kim, B. Chen, L. Guo, M. Llaguno, J. V. Hollingsworth, D. S. King, S. F. Banani *et al.*, "Phase transitions in the assembly of multivalent signalling proteins," Nature **483**(7389), 336–340 (2012).
[70] R. Laghmach, I. Alshareedah, M. Pham, M. Raju, P. R. Banerjee, and D. A. Potoyan, "RNA chain length and stoichiometry govern surface tension and stability of protein-RNA condensates," Iscience **25**(4), 104105 (2022).
[71] E. J. Carr, J. M. Ryan, and M. J. Simpson, "Diffusion in heterogeneous discs and spheres: New closed-form expressions for exit times and homogenization formulas," J. Chem. Phys. **153**(7), 074115 (2020).
[72] D. T. Gillespie, "A general method for numerically simulating the stochastic time evolution of coupled chemical reactions," J. Comput. Phys. **22**, 403–434 (1976).
[73] T. K. Sherwood, in *Transport Phenomena*, edited by R. Byron Bird, W. E. Stewart, and E. N. Lightfoot (John Wiley, New York, London, 1960), Vol. 780, pp. 13–75.
[74] A. Baer, S. E. Wawra, K. Bielmeier, M. J. Uttinger, D. M. Smith, W. Peukert, J. Walter, and A.-S. Smith, "The Stokes–Einstein–Sutherland equation at the nanoscale revisited," Small **20**(6), 2304670 (2024).
[75] D. T. Gillespie, "Exact stochastic simulation of coupled chemical reactions," J. Phys. Chem. **81**(25), 2340–2361 (1977).
[76] Y. Cao, D. T. Gillespie, and L. R. Petzold, "Avoiding negative populations in explicit Poisson tau-leaping," J. Chem. Phys. **123**(5), 054104 (2005).
[77] C. Mortici, "A new fast asymptotic series for the gamma function," Ramanujan J. **38**(3), 549–559 (2015).
[78] T. G. Kurtz, "The relationship between stochastic and deterministic models for chemical reactions," J. Chem. Phys. **57**(7), 2976–2978 (1972).
[79] G. Guigas and M. Weiss, "Sampling the cell with anomalous diffusion—The discovery of slowness," Biophys. J. **94**(1), 90–94 (2008).

[80] T. A. Waigh and N. Korabel, "Heterogeneous anomalous transport in cellular and molecular biology," Rep. Prog. Phys. **86**(12), 126601 (2023).
[81] Y.-q. Ma and J.-w. Liu, "The competing Glauber and Kawasaki dynamics induced phase transition in the ferromagnetic Ising model," Phys. Lett. A **238**(2–3), 159–163 (1998).
[82] F. Den Hollander, F. Nardi, E. Olivieri, and E. Scoppola, "Droplet growth for three-dimensional Kawasaki dynamics," Probab. Theory Relat. Fields **125**(2), 153–194 (2003).
[83] J. Wang, S. Kudesia, D. Bratko, and A. Luzar, "Computational probe of cavitation events in protein systems," Phys. Chem. Chem. Phys. **13**(44), 19902–19910 (2011).
[84] D. Qin, Z. He, P. Li, and S. Zhang, "Liquid-liquid phase separation in nucleation process of biomineralization," Front. Chem. **10**, 834503 (2022).
[85] Y. Iida, S. Hiraide, M. T. Miyahara, and S. Watanabe, "Solute interaction-driven and solvent interaction-driven liquid–liquid phase separation induced by molecular size difference," J. Chem. Phys. **160**(4), 044504 (2024).
[86] M. Naz, L. Zhang, C. Chen, S. Yang, H. Dou, S. Mann, and J. Li, "Self-assembly of stabilized droplets from liquid–liquid phase separation for higher-order structures and functions," Commun. Chem. **7**(1), 79 (2024).
[87] A. A. M. André and E. Spruijt, "Liquid–liquid phase separation in crowded environments," Int. J. Mol. Sci. **21**(16), 5908 (2020).